DYNAMIC PROPERTIES OF S-200-E BERYLLIUM

by
D. R. Christman
F. J. Feistmann

Materials and Structures Laboratory
Manufacturing Development, General Motors Corporation
General Motors Technical Center, Warren, Michigan 48090

DNA 2735F
MSL 71-23
1972, February

DYNAMIC PROPERTIES OF S-200-E BERYLLIUM

"This work was supported by the Defense Nuclear Agency under NWER Subtask AA 106"

by

D. R. Christman
F. J. Feistmann

Materials and Structures Laboratory
Manufacturing Development, General Motors Corporation
General Motors Technical Center, Warren, Michigan 48090

Prepared For

DIRECTOR
Defense Nuclear Agency
Washington, D.C. 20305

Under Contract DASA01-68-C-0114

ABSTRACT

Results of an experimental study on the dynamic properties of S-200-E beryllium are presented. Areas studied included uniaxial stress behavior, elastic constants, equation of state, elastic precursor decay, and shock wave profiles. The material showed a yield "plateau" and then significant strain hardening, and exhibited strain rate sensitivity. Longitudinal and shear wave velocities at 20°C were 12.84 and 8.86 mm/μsec. The shock wave equation of state up to 30 kb was determined to be linear: $\sigma_H = 0.7 + 152.7\ u_p$. Compressive wave tests showed a ramped, non-steady-state elastic precursor, and shock wave profiles showing both release behavior and attenuation were obtained. Scanning microfractographs were taken of spall fracture surfaces.

TABLE OF CONTENTS

LIST OF ILLUSTRATIONS

LIST OF ILLUSTRATIONS (Continued)

LIST OF TABLES

INTRODUCTION

This study of S-200-E beryllium was conducted under the PREDIX program initiated by the Defense Nuclear Agency[1]. In addition to beryllium, the program included studies of 6061-T6 aluminum[2], alpha titanium[3], OFHC copper[4], tantalum[5], and poly(methylmethacrylate)[6]. Beryllium was not studied under this program in as much detail as the other metals since a large amount of dynamic response data was already available in the literature.

The primary areas studied were: (1) uniaxial stress behavior; (2) elastic constants; (3) equation of state; (4) elastic precursor decay; and (5) shock wave profiles. The experimental techniques utilized in this study are reviewed in Reference 7. Briefly, the principal techniques were:

Stress-Strain Studies - A laboratory-type universal testing machine was used for uniaxial stress tests.

Elastic Constants - A pulse transmission overlap method was used for measuring longitudinal and shear wave velocity.

Equation of State - Gun-launched, flat-plate impact techniques were used to generate uniaxial strain conditions. Velocities up to 0.5 mm/μsec were achieved with a 102 mm single-stage compressed-gas gun, and hugoniot data were obtained with x-cut quartz gages.

Wave Propagation - Flat-plate impact techniques were also used. Wave profiles were measured with x-cut quartz gages and a laser velocity interferometer.

MATERIAL PROPERTIES

The beryllium tested had the designation S-200-E, Type 1, and was purchased from the Brush Beryllium Company. The specification sheets describing this grade of beryllium and its acceptance standards are given in Appendix A. All test specimens were machined from the same billet, identified as Lot No. 8494, and material certification is given in Table I. Shock wave test specimens were machined in the form of discs with the disc axis (and therefore shock wave propagation direction) parallel to the pressing direction. In addition, orthogonal specimens were machined for metallographic observation and ultrasonic measurement. Density determined for several specimens was 1.850 ± 0.002 g/cc. Hardness was measured as $52R_A$ and $65R_G$.

Grain structure of the material is shown in Figure 1. There was little evidence of structure or texturing due to the pressing and sintering operation, however, there may have been crystallographic anisotropy which would not be detected by conventional photomicrography. The as-received material, when suitably prepared to eliminate machining and polishing artifacts, showed a generally equiaxed structure (10-20 μm grain size) with almost no evidence of twins.

Dilatational (longitudinal) wave velocity was measured in the pressing direction (Z) and orthogonal or transverse to the pressing direction (X and Y), at 1 MHz. Shear (transverse) wave velocity measurements were made at 5 MHz. Results, including elastic constants calculated assuming isotropic behavior were:

TABLE I - S-200-E BERYLLIUM CERTIFICATION

THE BRUSH BERYLLIUM COMPANY

Cleveland, Ohio • Elmore, Ohio • Hayward, California

MATERIAL CERTIFICATION

Customer: GM Corporation
GM Technical Center
12 Mile and Mound Roads
Warren, Michigan 48090

Date: June 16, 1971
S.O.#: D 999
P.O.#: MD 7105755
Specification: S-200-E, Type I

Material Description:

Lot No. 8494, One (1) Beryllium Disc No. A-1 from Sketch No. II
Lot No. 8494, One (1) Beryllium Disc No. B-1 from Sketch No. II
Lot No. 8494, One (1) Beryllium Disc No. C-1 from Sketch No. II

CHEMICAL COMPOSITIONS: (Wt.%)	
ELEMENT	Lot No. 8494
Be	98.55
BeO	1.39
C	.07
Fe	.10
Al	.02
Mg	.004
Si	.03
OTHER ELEM. EA.	-.04
OTHERS TOTAL	

MECHANICAL PROPERTIES					
DIR.	FTU	FTY	%EL		
Lot 8494					
Trans.	57,900	38,200	4.9		
Trans.	56,100	38,700	4.1		

DENSITY gm/cc	AVG GRAIN SIZE: (Microns)
1.85	10.3 Microns
RADIOGRAPHIC INSP. PER: MIL-STD-453	PENETRANT INSP. PER: MIL-I-6866
ADDITIONAL INFORMATION:	

This is to certify that the above material satisfies the requirements of Specification S-200-E, Type I Drawing No. II Purchase Order MD 7105755 and was removed from Pressing No. 8494.

J.J. Jesberger/lel
THE BRUSH BERYLLIUM COMPANY
QUALITY CONTROL

cc:
Shipping (3) Sales (1) File (1)

53677-218 3/71

MSL-71-23

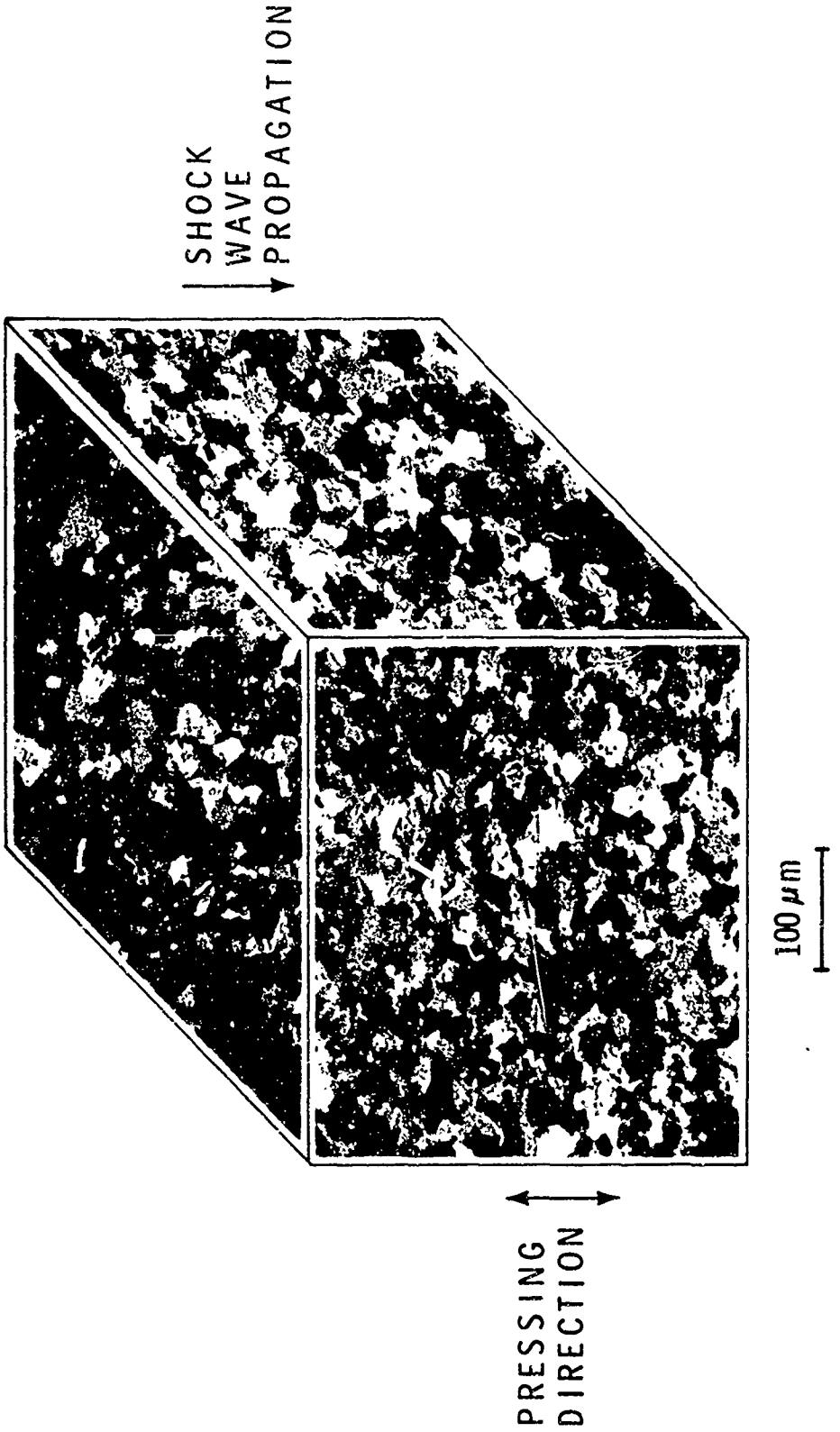

Figure 1 S-200-E Beryllium Grain Structure

	Pressing Direction (Z)	Orthogonal Direction (Average of X & Y)
Dilatational Wave Velocity (mm/μsec):	12.84±0.04	12.57±0.1
Shear Wave Velocity (mm/μsec):	8.86±0.04	8.82±0.1
Shear Modulus (kbar):	1453	1440
Bulk Modulus (kbar):	1114	1005
Young's Modulus (kbar):	3038	2923
Lamé's Parameter (kbar):	145.6	44.8
Poisson's Ratio:	0.046	0.015

The data indicated there is some elastic anisotropy between the pressing and orthogonal directions, with significant differences in calculated values for Lamé's parameter and Poisson's ratio.

Although temperature and pressure dependence of elastic wave velocities was not determined for this beryllium, Silversmith and Averbach[8] and Voronov and Verseshchagin[9] have reported data on pressure dependence of elastic constants for beryllium and Baldwin[10] has reported temperature dependence data.

Values for the Gruneisen parameter and Debye temperature at 25°C were calculated, using thermal expansion and specific heat data taken from the literature:[11-14]

Volume coefficient of thermal expansion, β:

$$34 \times 10^{-6} + 0.02 \times 10^{-6} T \quad /°C$$

Specific heat, c_p:

$$0.40 + 0.001 T \quad cal/g-°C$$

Gruneisen parameter, γ_0:

$$\gamma_0 = \frac{\beta K_0^S}{\rho_0 c_p}$$

where K_0^S is bulk modulus,

$$\gamma_0 = \frac{34 \times 10^{-6} \times 1114}{1.85 \times 0.40} \times 23.9 = 1.22$$

Debye temperature

$$\Theta = \frac{h}{k}\left(\frac{9N}{4\pi V}\right)^{1/3}\left(\frac{1}{C_L^3} + \frac{2}{C_S^3}\right)^{1/3}$$

where h is Planck's constant, k is Boltzmann's constant, N is number of mass points and V is sample volume.

$$\Theta = 4.3 \times 10^{-5}\left(\frac{N}{V}\right)^{1/3}\left(\frac{1}{C_L^3} + \frac{2}{C_S^3}\right)^{-1/3}$$

Θ = 1430 °K

for N = 2 (atoms per unit cell),
Ω^* = 16.2 x 10^{-21} mm^3, C_L = 12.84 mm/μsec
and C_S = 8.86 mm/μsec.

* The unit cell volume = 0.866 a^2c, where a = 2.2856Å and c = 3.584Å.[15]

UNIAXIAL STRESS BEHAVIOR

The deformation behavior of various grades of beryllium has been extensively studied and the reader is referred to References 16 to 24 for details of some of the more recent work. For the subject beryllium, uniaxial stress tests were conducted in compression at two strain rates and under reverse loading conditions. Results of the compression tests are given in Figure 2 and show a well-defined yield with no strain hardening out to a few-tenths percent strain (depending on strain rate) and then significant strain hardening at larger strains. For an increase in strain rate from 0.2×10^{-3} sec to 0.2 sec, the yield and flow stress increased about 15%.

Results of the reverse loading or Bauschinger effect* tests are given in Figures 3 and 4. In these tests, the specimens were first loaded in compression until some specified strain was reached and then immediately reloaded into tension. A different specimen was used for each test, and in one case (see Figure 4) the reloading strain rate was about a factor of ten higher then the initial loading rate. There was no indication of the yield "plateau" upon reloading and the reverse loading curve became slightly steeper and higher with increasing plastic prestrain. Note that the specimens prestrained to 2% and 3% fractured at less than 2% strain in tension. This is significantly lower than the 4 to 5% tensile

* The Bauschinger effect can be defined as the reduction in stress at a given strain in the reverse direction compared to that in the original loading direction.

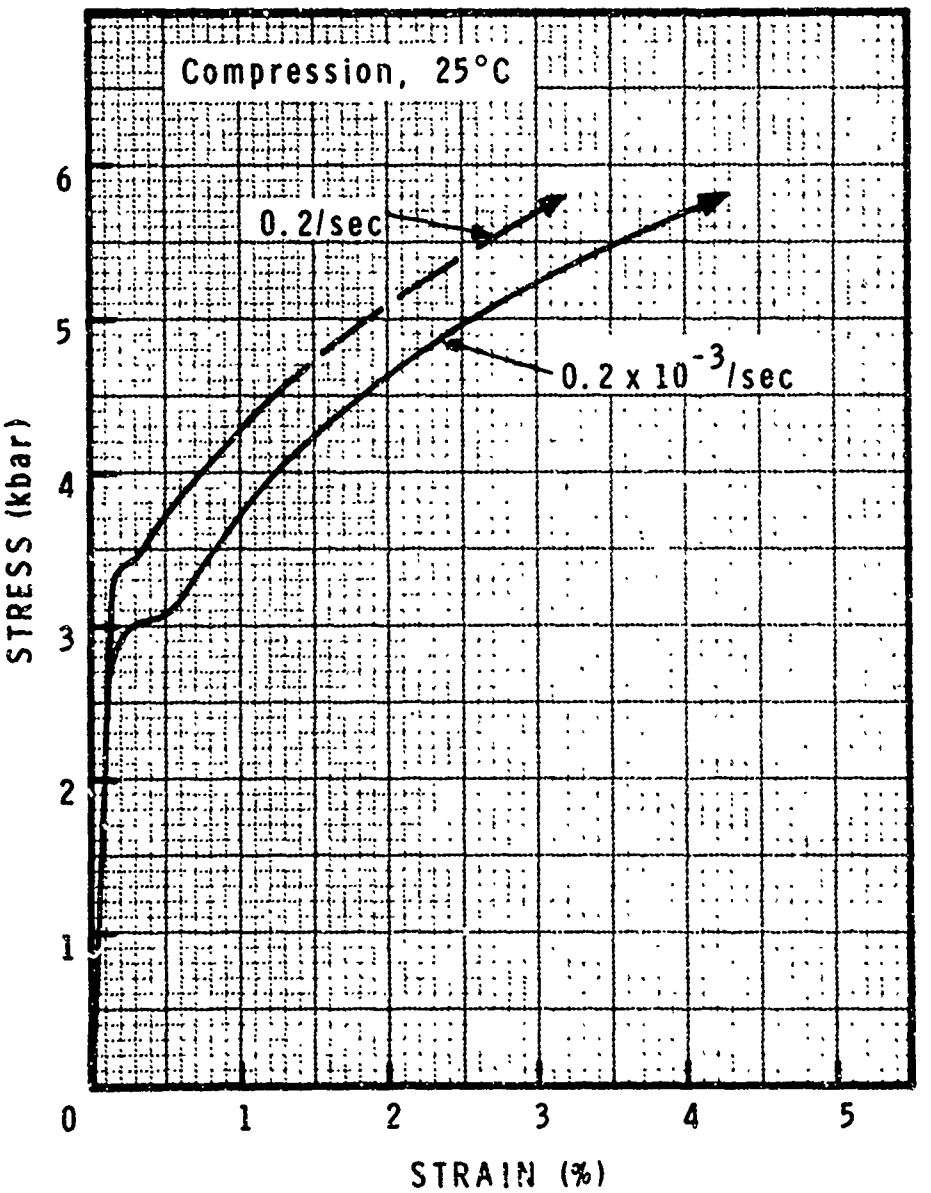

Figure 2 Compressive Stress vs. Strain, S-200-E

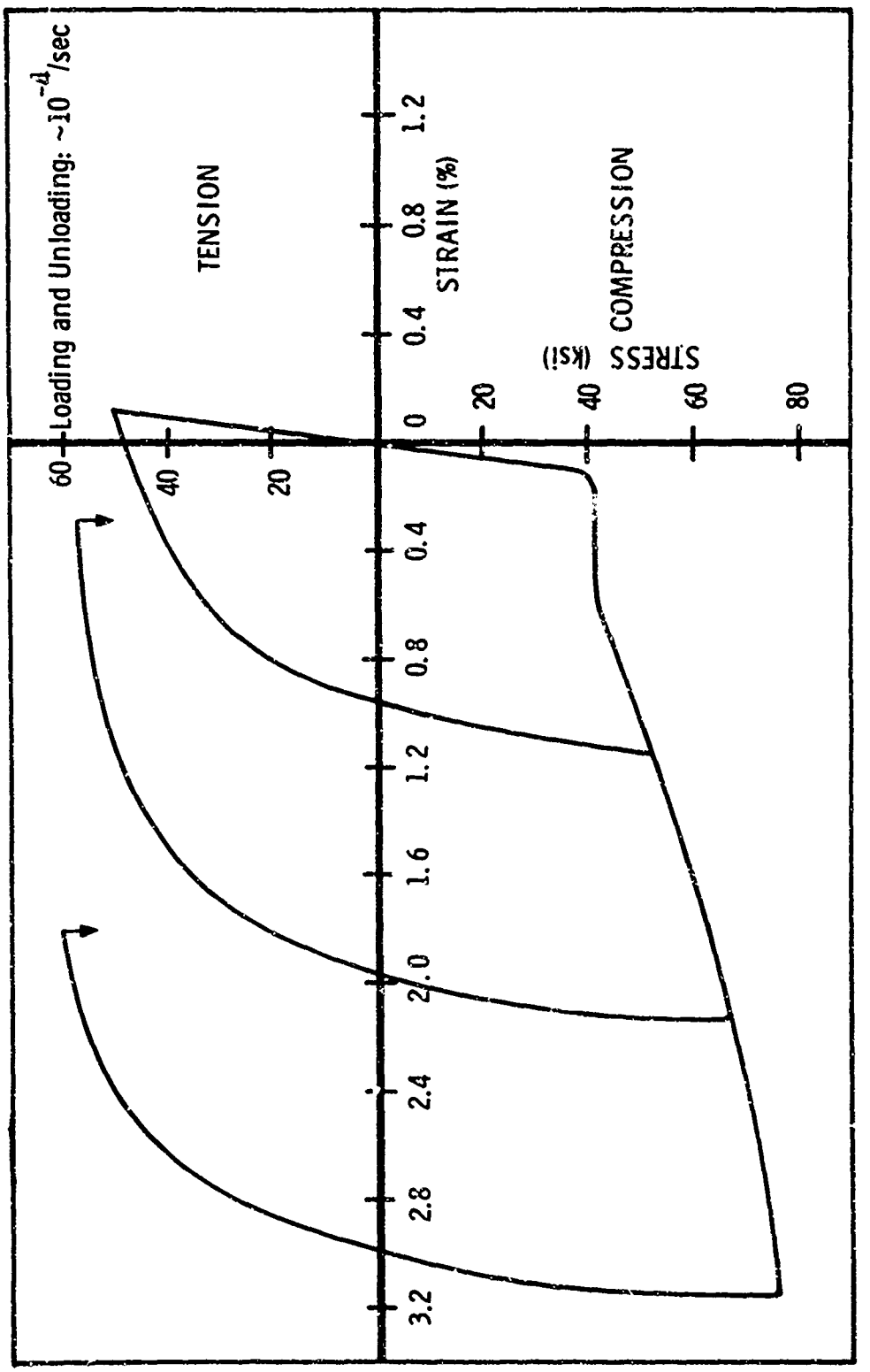

Figure 3 Reverse Loading Behavior, Strain Effects, S-200-E

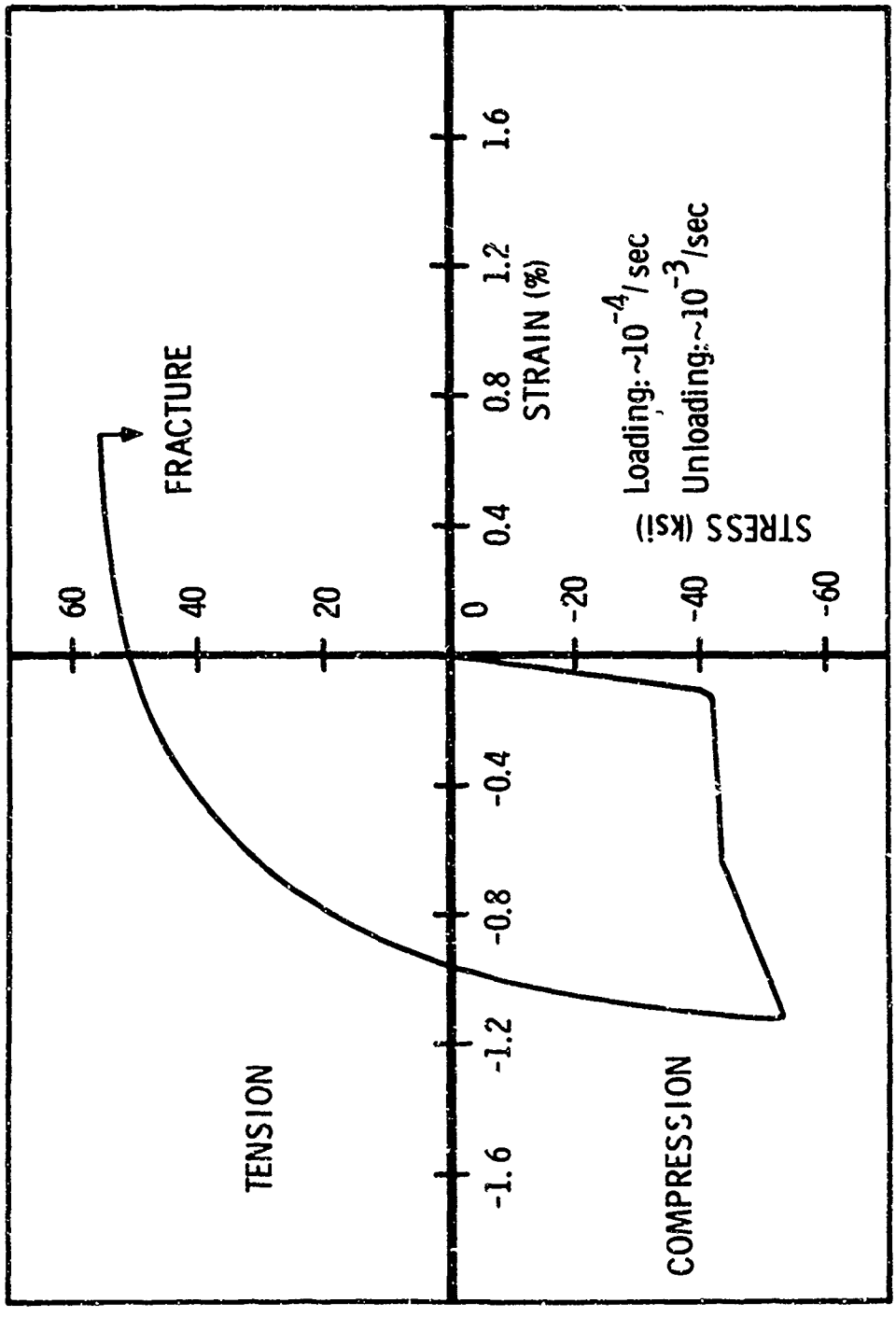

Figure 4 Reverse Loading Behavior, Rate Effects, S-200-E

strain-to-fracture reported in the material certification (Table I). There was a small strain rate effect on reloading as indicated by the slight increase in flow stress at the higher rate indicated in Figure 4.

EQUATION OF STATE

Several tests were conducted to determine the low pressure equation of state for this beryllium for use in wave propagation calculations. Considerable work had been done previously on S-200-E and other grades of beryllium (see, e.g., References 25-29), and much of this work has been summarized in a review by Davison and Johnson[30]. Equation of state data was obtained with x-cut quartz gages, and a representative direct impact record is shown in Figure 5. Note that there is a slight stress-relaxation in the first 50 nsec and it was the relaxed stress level that was used as the equilibrium hugoniot point. Also shown in Figure 5 are representative wave profile records from a quartz gage test and a velocity interferometer test. These results are discussed later in this report.

The equation of state for S-200-E beryllium for 3 to 30 kbars was determined as:

$$\sigma_H = 0.7 + 152.7\, u_p \qquad (1)$$

where σ_H is hugoniot stress (kbar) and
u_p is particle velocity (mm/μsec).

Equation 1 was obtained by doing a least squares fit to the six data points shown in Figure 6. Two of these points were taken from Froula's earlier work on S-200 beryllium[25]. A linear $\sigma_H - u_p$ relation gave the best fit to the data and had a standard error of 0.6 kbar. Estimated error for the data points was ± 2% for σ_H and ± 1% for u_p.

MSL-71-23

TIME →

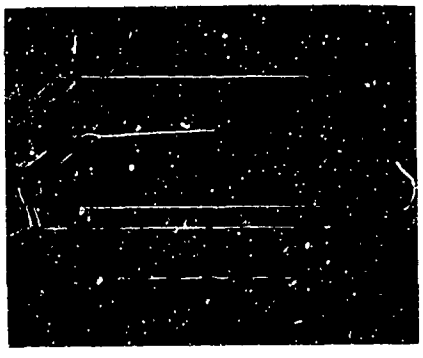

QUARTZ DIRECT IMPACT
(Buffered)

Be → WC/Qz
V_I = 0.1484mm/μsec
σ_H = 20 kbar

QUARTZ TRANSMITTED WAVE

Al → Be/Qz
V_I = 0.1501mm/μsec
X = 9.15mm
σ_H = 12 kbar

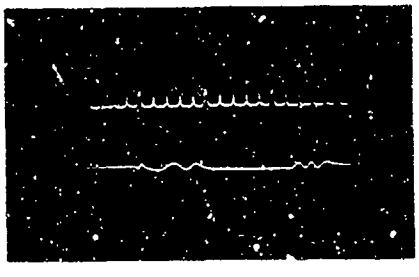

VELOCITY INTERFEROMETER

FQ → Be/FQ
V_I = 0.1538mm/μsec
X = 6.172mm

Figure 5 Experimental Records, Quartz Gage and Velocity Interferometer, S-200-E

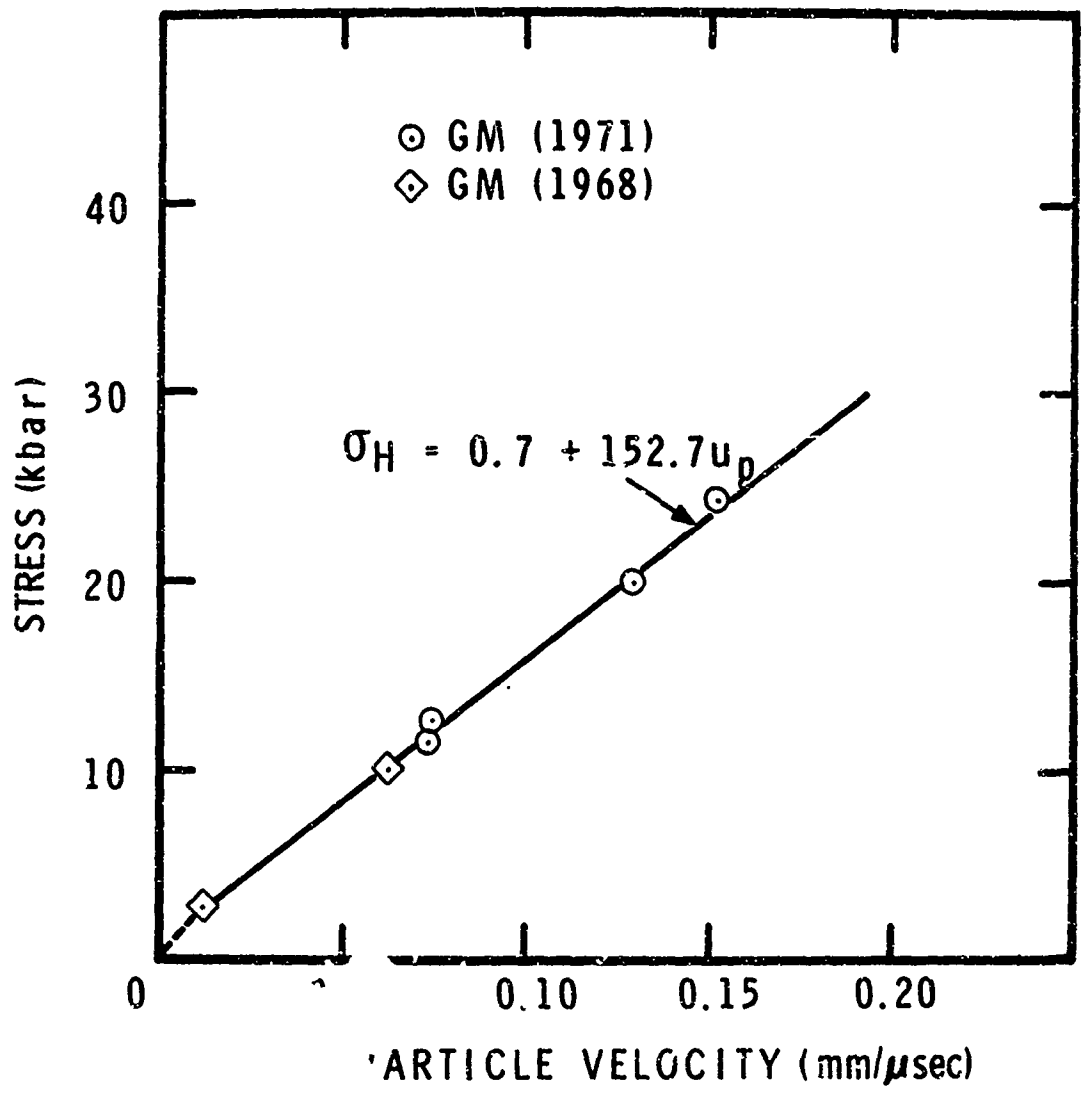

Figure 6 Stress-Particle Velocity Hugoniot, S-200-E

The stress-compression and mean pressure-compression response was calculated from Equation 1 by assuming an ideal elastic-plastic wave structure with equilibrium initial and final states and applying mass and momentum conservation equations. This gave:

$$\sigma_H = 1.3 + 1220\ \mu$$
$$P_H = 1220\ \mu \qquad (2)$$

where P_H is hydrostatic pressure (kbar) and μ is compression $\left(\frac{v_0}{v} - 1\right)$.

The hydrostat ($P_H - \mu$) was obtained by subtracting the stress-axis intercept value from the $\sigma_H - \mu$ equation. This approach satisfies the requirement that the $P_H - \mu$ function pass through zero but assumes the deviatoric stress component (σ_D) constant at 1.3 kbar, i.e., no strain hardening. A more rigorous treatment would treat σ_D as a function of strain and would include consideration of anisotropic effects.

The linear form of Equations 1 and 2 implies a constant plastic wave velocity which was calculated to be 8.25 mm/μsec. Although it is recognized that actual material response does not satisfy exactly an ideal elastic-plastic structure with constant shock velocity, this assumption is considered justified for the relatively small range in stress (3 to 30 kbar) to which it has been applied. Also for this stress range, the plastic wave is so ramped as to make consideration of whether shock velocity is constant or a function of particle velocity an academic point.

For comparison, the hydrostat as determined from ultrasonics data[8] is

$$P_H = 247\ [(1 + \mu)^{4.5} - 1] \qquad (3)$$

(Murnaghan equation of state)

and from hydrostatic compression data[10] is

$$\frac{\mu}{1+\mu} = 0.977 \times 10^{-3}\ P_H - 3.92 \times 10^{-6}\ P_H^2 \qquad (4)$$

(For stresses up to 30 kbar, the corrections from isothermal or isentropic conditions to the hydrostat are less than 1% and have been neglected).

The hydrostat as determined from Equations 2 to 4 is shown in Figure 7. The shock wave hydrostat is slightly higher than the ultrasonics or hydrostatic compression curves, however, inclusion of strain hardening and other effects in obtaining $P_H - \mu$ from $\sigma_H - u_p$ would reduce this difference.

Since twinning can be an important deformation mode in beryllium[31], several recovered specimens were examined metallographically and are compared to the as-received material in Figure 8. There were almost no twins visible in the as-received material or after shocking to 12 kbars. At 24 kbars, however, twinning is observed, although affecting only a few percent of the observed area.

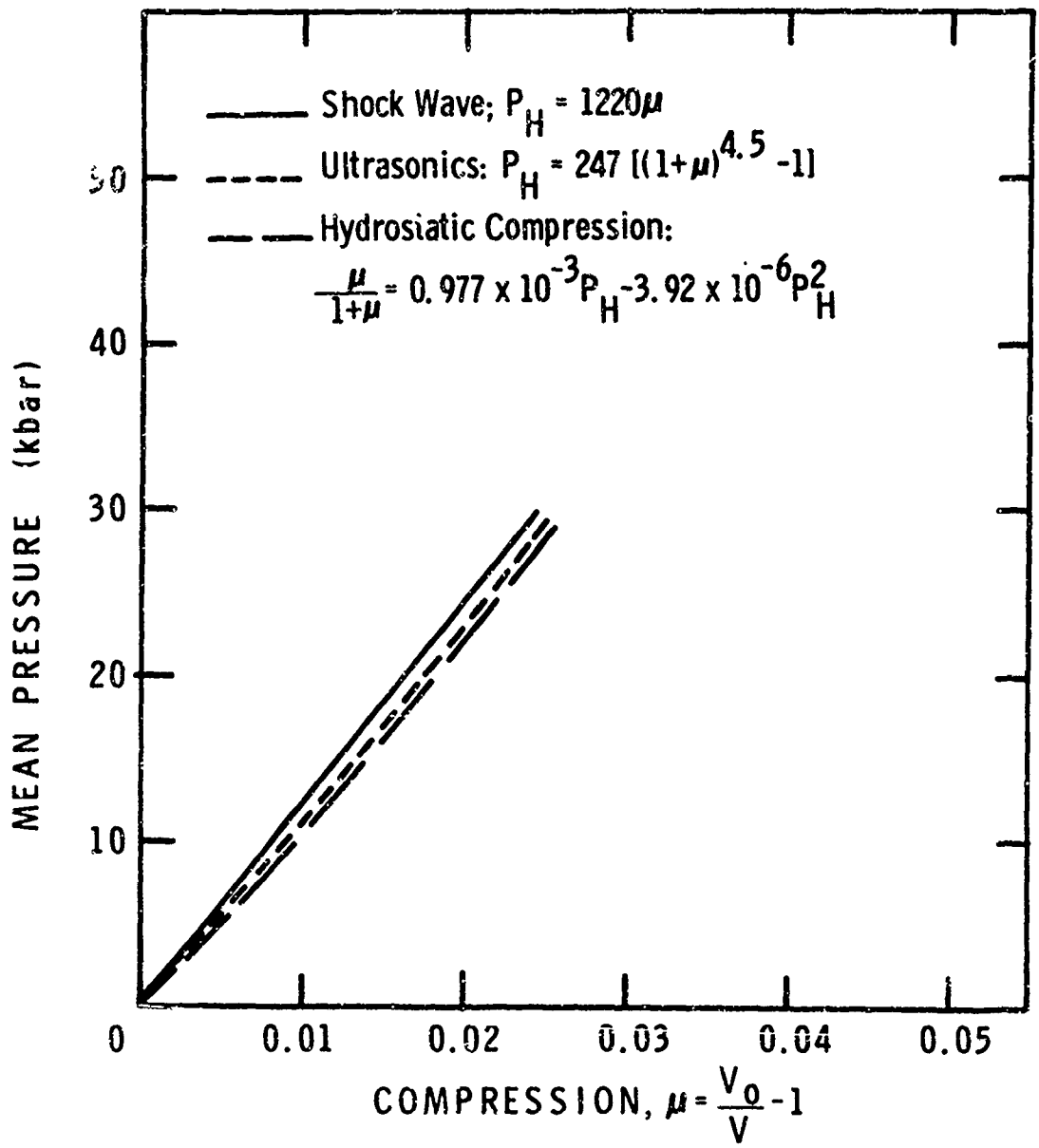

Figure 7 Mean Pressure-Compression Hydrostat, Beryllium

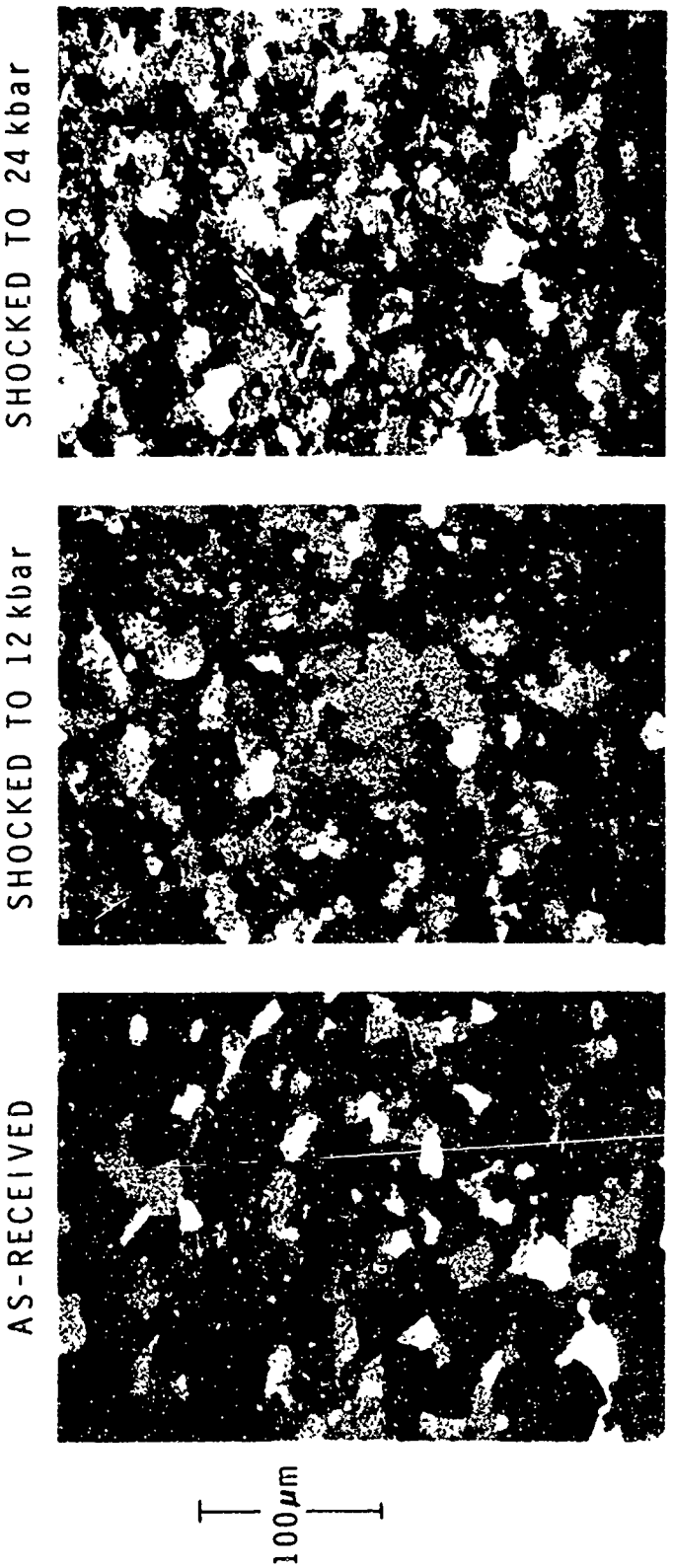

Figure 8 As-Received and Shock-Loaded Microstructure, S-200-E

WAVE PROPAGATION

COMPRESSIVE WAVES

Compressive wave tests were carried out using x-cut quartz gages, primarily to determine elastic precursor decay behavior. Data of this type is useful in evaluating certain parameters in dislocation models of compressive wave development (see e.g., Refs. 32 and 33). Results for S-200-E beryllium are shown in Figure 9. The elastic wave shows a rise-time greater than can be attributed to experimental effects, such as tilt. This behavior has been reported for other grades of beryllium,[26,34] for uranium,[34] and for copper.[4,34] Although a ramped elastic wave seems characteristic of polycrystalline beryllium, single-crystal beryllium shows a fast-rising elastic wave with about a factor of 10 variation in precursor level depending on crystal orientation (with propagation along the c-axis giving the highest value).[34] This anisotropy could contribute to smearing or spreading of the elastic wave front in a polycrystalline material with randomly oriented grains.

The initial elastic stress level (at impact) was $\sim$ 15 kbar and has decayed $\sim$ 65% by 1.74 mm. Although the yield in uniaxial strain is not well-defined, the precursor continues to decay at longer propagation distances and appears to be approaching an equilibrium or steady-state elastic limit of 3 to 4 kbar. For comparison, the hugoniot elastic limit can also be estimated from uniaxial stress data and from the elastic and plastic hugoniots:

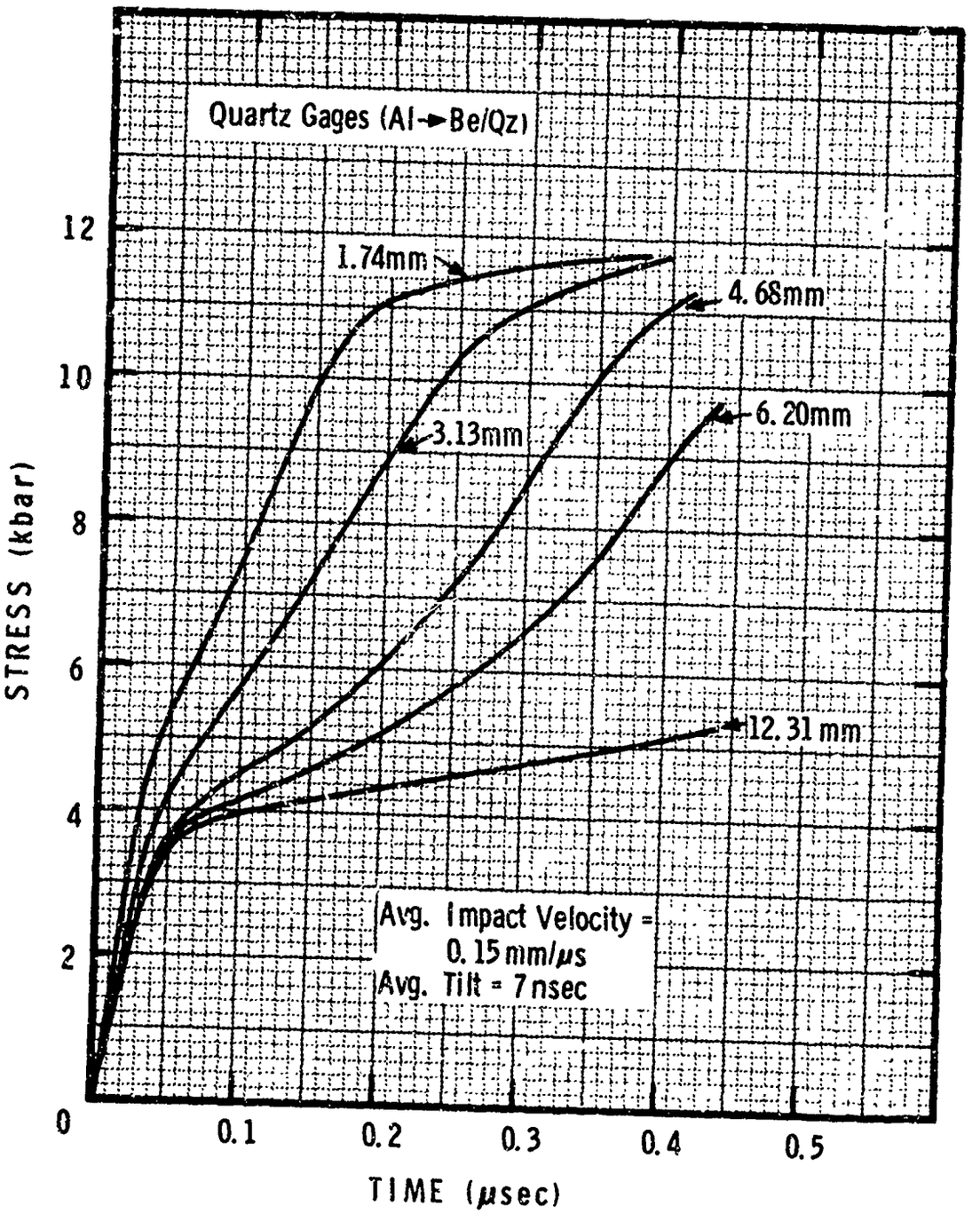

Figure 9 Elastic Precursor Development, S-200-E

A. Uniaxial Stress

$$\sigma_e = \sigma_\sigma \left(\frac{1-\nu}{1-2\nu}\right) \tag{5}$$

where σ_e is hugoniot elastic limit, σ_σ is yield in uniaxial stress, and ν is Poisson's ratio.

Strain Rate (Sec^{-1})	σ_e (kbar)
0.2×10^{-3}	3.2
0.2	3.6

B. Hugoniots

$$10\ \rho_0\ C_L\ u_e = A + Bu_e \tag{6}$$

where u_e is particle velocity at the elastic limit.

Solving for u_e gives:

$$u_e = 0.0083 \text{ mm/}\mu\text{s}$$

$$\therefore \sigma_e = 2.0 \text{ kbar}$$

Complete compressive wave development is shown in Figure 10 for two propagation distances. The ramped elastic wave is evident, as well as spreading of the plastic wave which indicates steady-state wave behavior has not been achieved. The arrows in Figure 10 indicate calculated plastic wave arrival time, assuming a shock velocity of 8.25 mm/μsec. Although

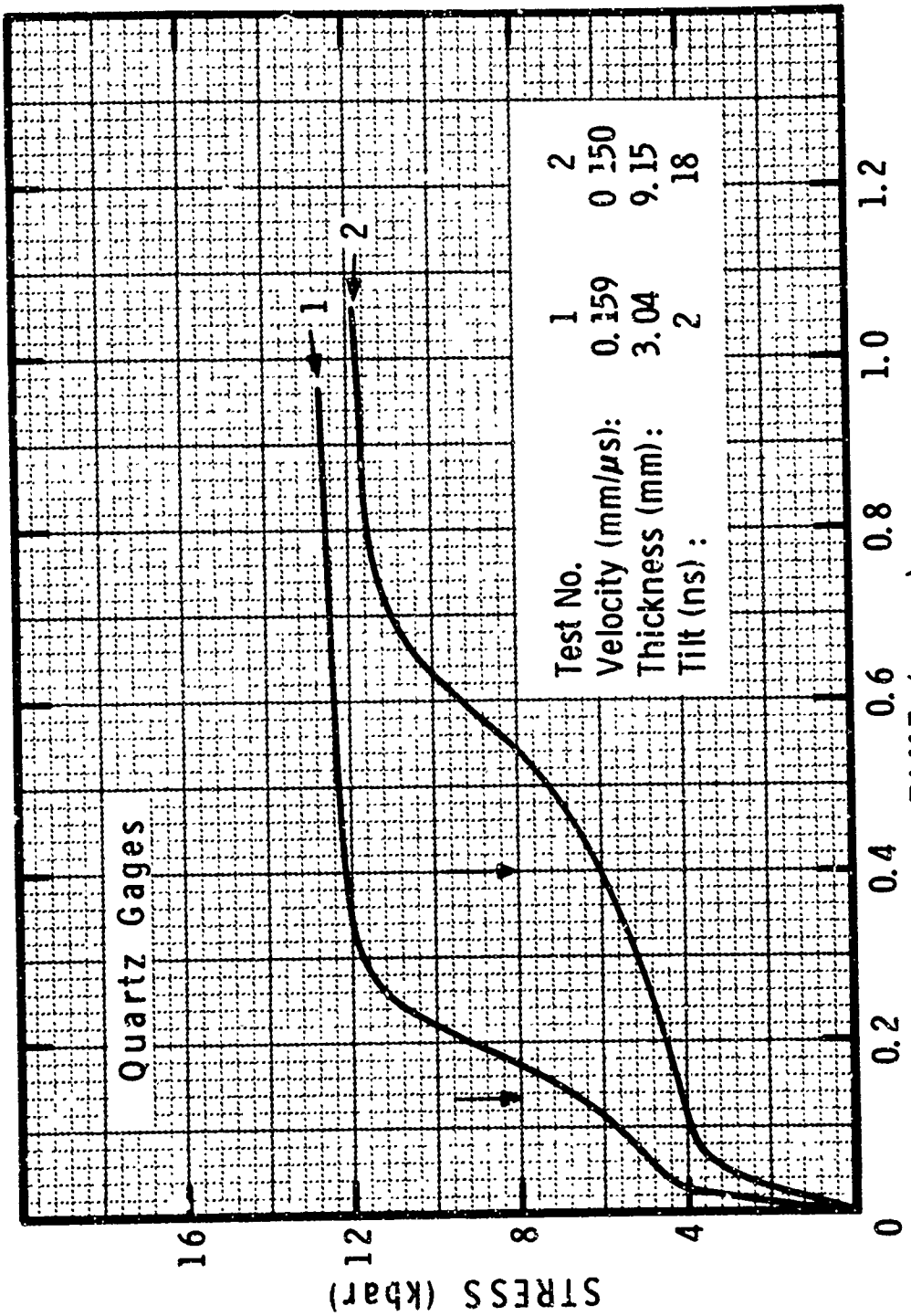

Figure 10 Compressive Waves, S-200-E

the calculated plastic wave velocity lies within the rise-time of the measured wave, the plastic wave is not a step pulse and shows spreading with propagation distance at this stress level. This means that transformation of the hugoniot from the $\sigma_H - u_p$ plane to $\sigma_H - \mu$ by assuming ideal elastic-plastic wave structure and steady-state conditions may lead to some uncertainty. The transit time for the elastic wave was measured on the 9.15 mm test and gave a velocity for the initial wave arrival of 12.8 ± 0.1 mm/μsec.

RELEASE WAVES AND ATTENUATION

Complete wave profiles were obtained using the laser velocity interferometer. All tests on S-200-E were carried out with fused quartz impactors. This gives a "square" input wave to the target, with a nearly instantaneous release* at the impactor-target interface. In order to provide a free surface on the rear of the impactor yet prevent fracture during acceleration, the fused quartz is supported by aluminum honeycomb. The contact area is ∿ 1% and is assumed to have a negligible effect on the release wave. A representative impactor and target assembly are shown in Figure 11. Note the honeycomb behind the fused quartz impactor. Also, the rear of the target is pictured, showing the fused quartz "window" and an aluminized spot at the target/window interface. Test conditions for all velocity interferometer tests are listed in Table II and the profiles are given separately in Appendix B for reference.

* The compressive wave is not released completely to zero, however, due to slight impedance differences between fused quartz and beryllium.

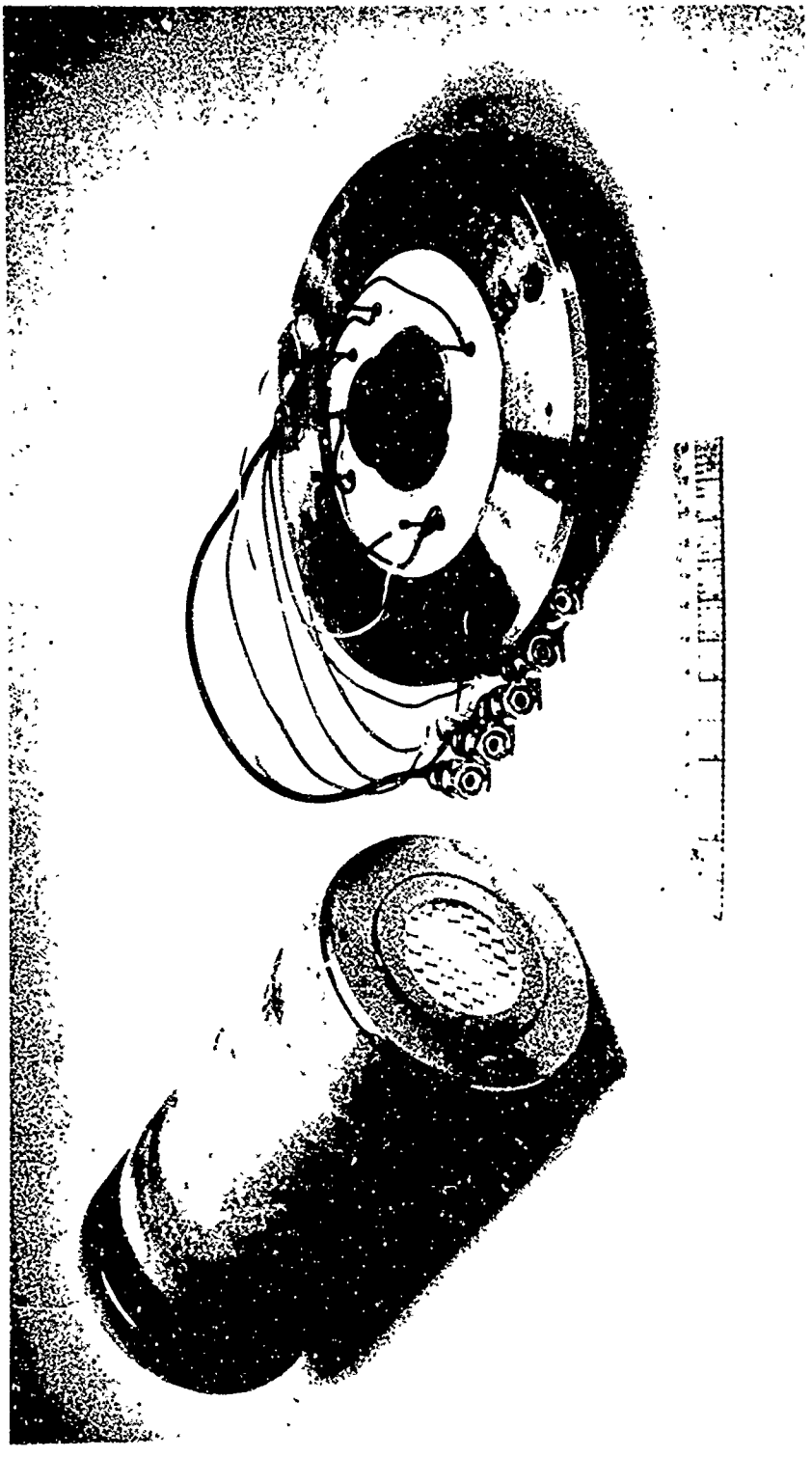

Figure 11 Impactor and Target Assembly, Showing "Window" on Rear of Target

TABLE II

VELOCITY INTERFEROMETER TEST DATA

Test No.	V_I Impact Velocity (mm/μsec)	Approx. Max. Stress (kbar)	X_0 Impactor Thickness (mm)	X Target Thickness (mm)	X/X_0	Configuration[1]
102[2]	0.1259	10	2.906	6.114	2.10	Al-Be/FQ
260	0.1558	11	3.200	6.172	1.93	FQ-Be/FQ
261	0.1735	12	3.200	3.228	1.01	FQ-Be/FQ
262	0.1590	11	3.226	12.28	3.81	FQ-Be/FQ
263	0.307	21	3.208	6.185	1.93	FQ-Be/FQ
264	0.0828	6	3.213	6.152	1.91	FQ-Be/FQ
265	0.1875	13	3.211	6.167	1.92	FQ-Be
266[2]	0.1677	12	3.051	6.096	2.00	FQ-Be
267	0.351	24	1.509	6.203	4.11	FQ-Be/FQ
268	0.346	24	1.524	9.149	6.00	FQ-Be/FQ
269	0.345	24	1.661	12.30	7.41	FQ-Be/FQ

[1] Al is 6061-T6 aluminum and FQ is fused quartz.

[2] High-purity beryllium target (see Reference 26), all others S-200-E beryllium targets.

Complete wave profiles are shown in Figure 12 for various propagation distances and impact velocities. Even with the high resolution velocity interferometer, the elastic wave rise-time is 40 to 80 nsec. The behavior of the elastic portion is not completely consistent, e.g., the level for Test No. 4 is lower but slightly steeper than for Test No. 1, yet both had the same propagation distance. Since the interferometer records were of good quality for these tests and interpretation was straight-forward, these differences are believed to be real and due to material effects which would include material variability. Also note the ramped top of the wave for Test No. 4. This is also believed to be a material effect although it is possible that a slight shift in light level of the reflected laser beam could cause similar behavior. The release wave is dispersive showing spreading with propagation distance, but does not have a distinct elastic-plastic structure.

Test No. 1 from Figure 12 is compared to a wave profile obtained for a high-purity beryllium in Figure 13. This high-purity (HP) beryllium had $\sim$ 0.03% BeO content and was supplied in the form of wrought plate. The material is described in detail in Reference 26. The principal differences in the response of the two materials are a more ramped and poorly-defined elastic wave and a ramped wave-top for the HP material.

Attenuated waves in S-200-E are shown in Figure 14. Again, the precursor levels are not entirely consistent. Although the amount of attenuation is relatively small (< 15%), these profiles should provide a reasonable check for models of compressive and release wave development and propagation.

MSL-71-23

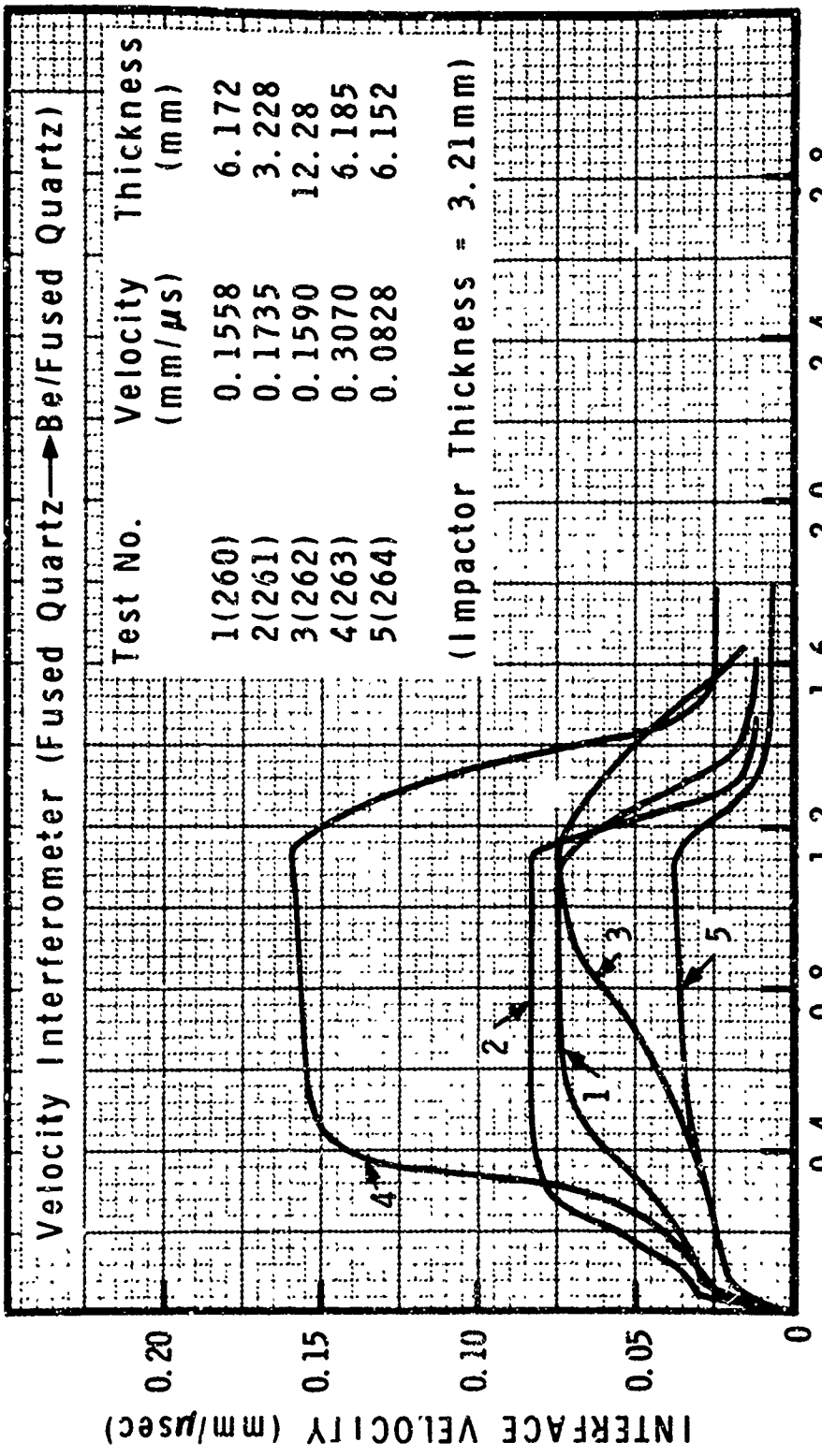

Figure 12 Complete Wave Profiles, S-200-E

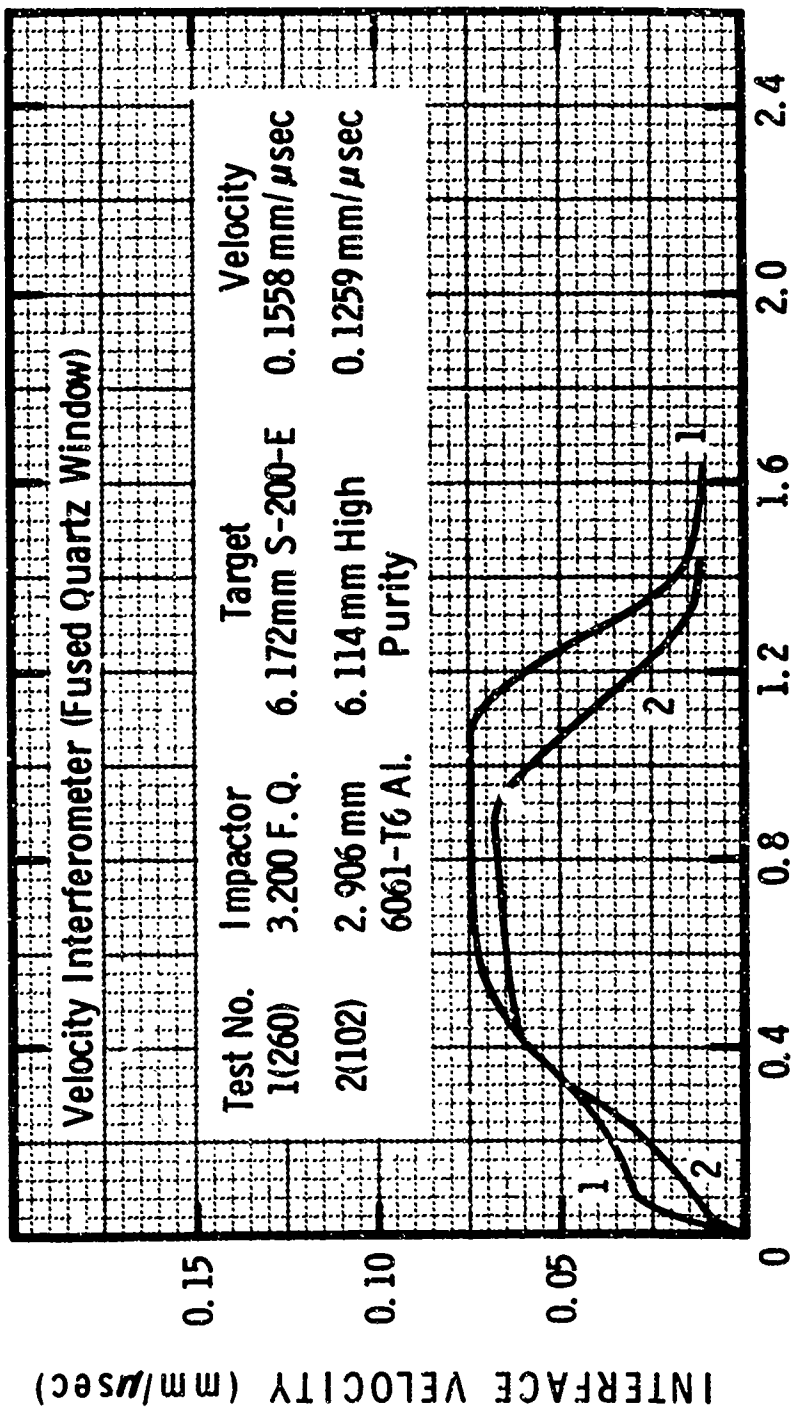

Figure 13 Complete Wave Profiles, Beryllium

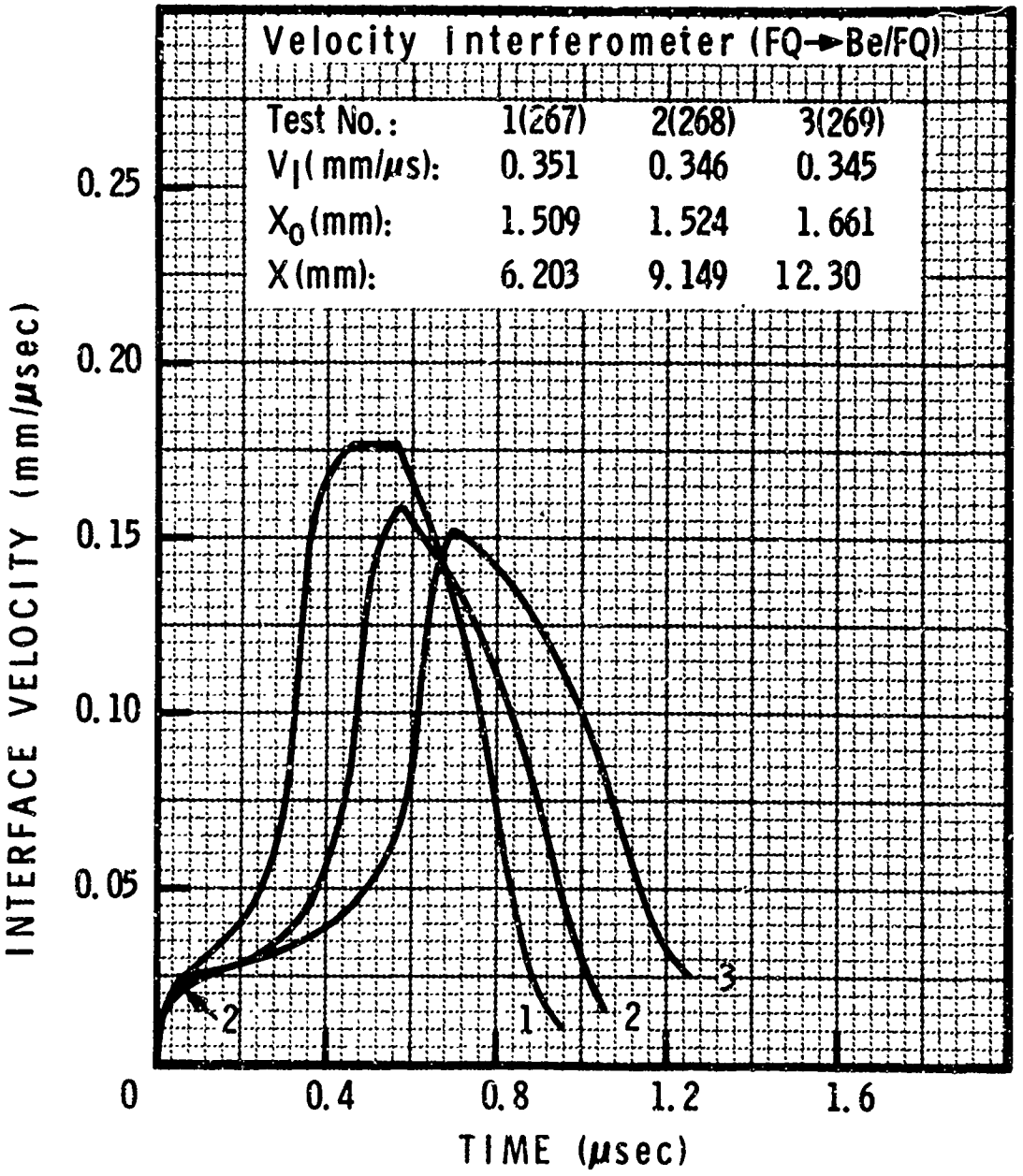

Figure 14 Wave Attenuation, S-200-E

FRACTURE

Fracture in beryllium was studied by measuring wave profiles under spall producing conditions and by examination of fracture surfaces with a scanning electron microscope. A detailed study of spall fracture in S-200 was carried out by Warnica[35] using target recovery and examination techniques, and no additional recovery-type tests were performed on the present beryllium. Spall data has also been reported for high-purity beryllium[26] and N50A beryllium[36].

Complete wave profiles showing spall fracture response are given in Figure 15 for S-200-E and high-purity (HP) berylliums. These tests had a fused quartz impactor and beryllium target configuration, with a free rear surface on the target for reflection of the compressive wave. Evidence of spall fracture is shown as a reversal of the release wave. The amount of pullback (decrease in free surface velocity to the point of first reversal) may be related to the spall strength of the material for a given impact geometry. An empirical relation for this was given by Taylor as:[34]

$$\sigma_S = \rho C \ (\Delta u_{fs}/2) \qquad (7)$$

where σ_S is spall strength, ρ and C are local density and longitudinal wave speed, and Δu_{fs} is pullback.

The data in Figure 15 gives $\sigma_S \approx 8$ kbar for S-200-E and $\sigma_S \approx 3.5$ kbar for HP, for these particular impact conditions. For comparison, the incipient spall velocities as estimated

MSL-71-23

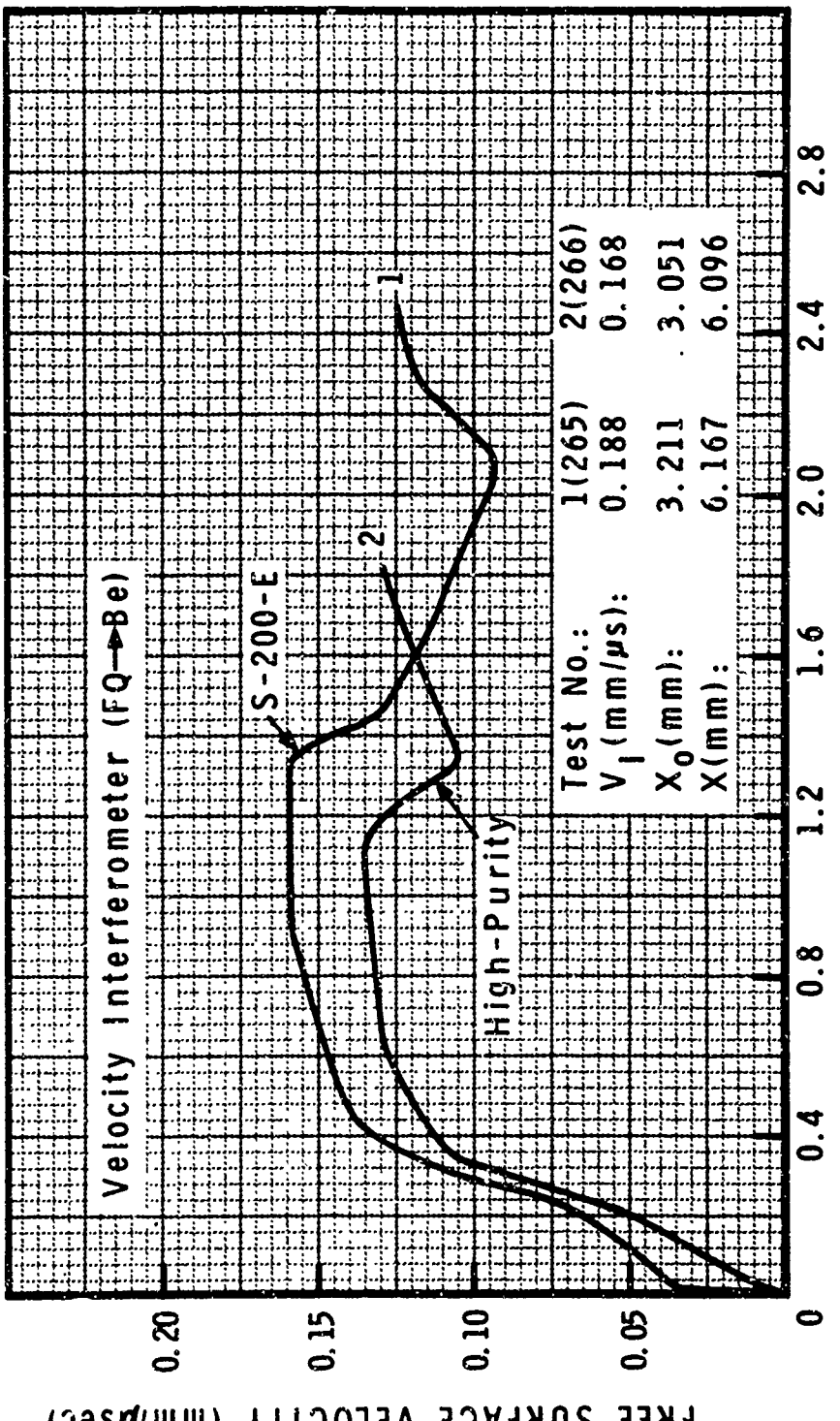

Figure 15 Spall Wave Profiles, Beryllium

from recovery test data* were ∿ 0.10 mm/μsec and ∿ 0.055 mm/μsec for S-200-E and HP respectively. The calculated spall strength is not constant for a given material since it is proportional to Δu_{fs}. This factor has been found to change with target temperature, pulse width, and pulse shape for 6061-T6 aluminum[37] and beryllium probably shows similar behavior. For the tests shown in Figure 15, the spall plane was ∿ 4.5 mm from the target rear surface.

Fracture surfaces for the S-200-E studied under the present program are shown in Figure 16 and 17**. The surface is essentially the same for a low strain rate test (Figure 16) and a high strain rate test (Figure 17), showing some evidence of plastic flow but with brittle fracture facets.

Fractured specimens were available from several previous beryllium studies,[25,26,35,36] and scanning microfractographs are shown in Figures 18 to 21. These specimens were from spall tests as well as equation of state tests where the target was recovered. HP beryllium (Figure 18) shows a brittle failure mode with almost no plastic flow. Fracture surfaces from HP, N50A, and S-200-E are compared in Figure 19, and show significant differences in terms of fracture facet size. The influence of target temperature on fracture surfaces in S-200-E and HP is shown in Figures 20 and 21. There appears to be a slight increase in "ductility" at 538°C for the S-200-E but no significant change at 260°C for either beryllium.

---

* The impact spall velocities could not be obtained directly since the recovery tests were for like-into-like conditions, i.e., beryllium-into-beryllium.

** The submicron particles visible in Figures 17 and 18 are contaminants from the recovery operation.

MSL-71-23

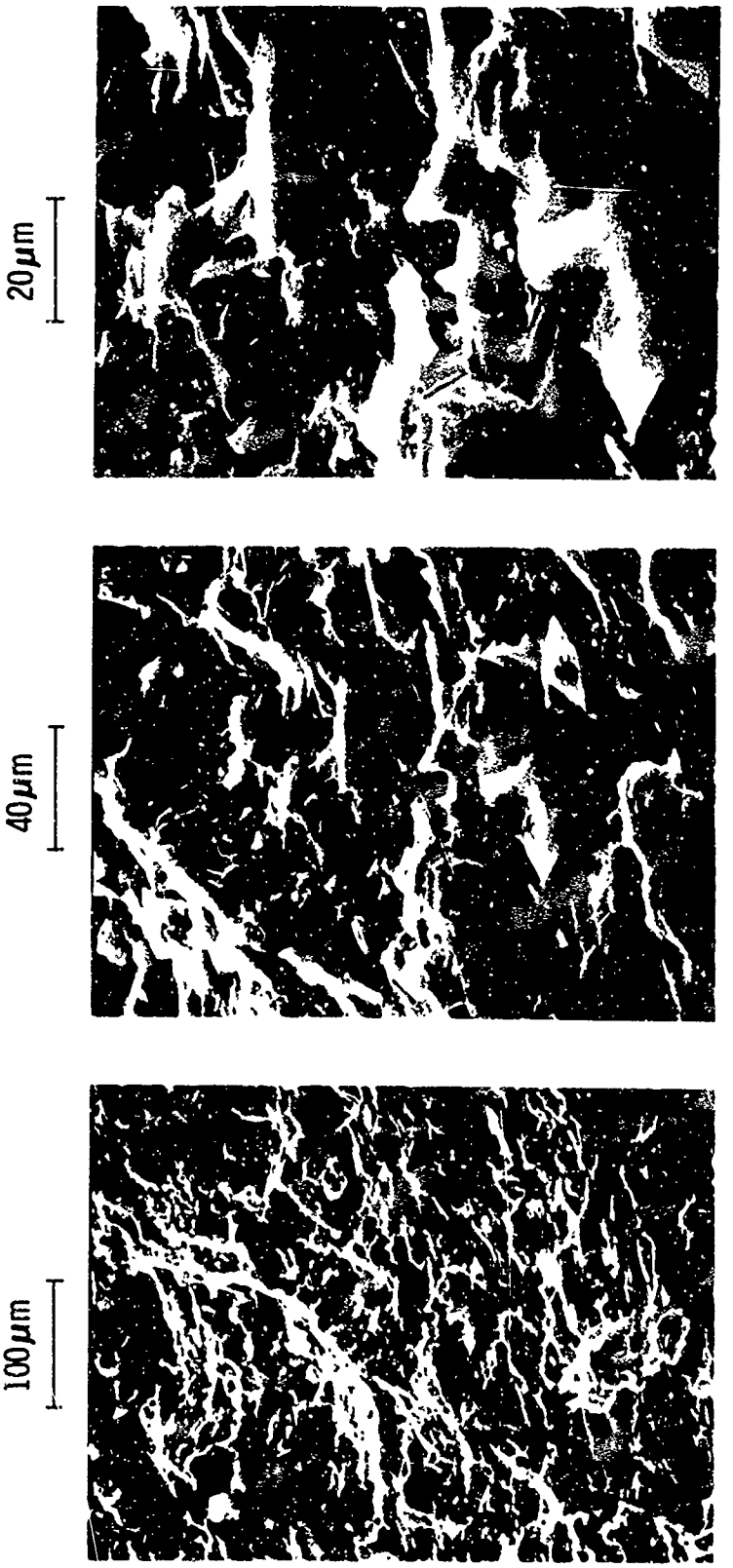

Figure 16 Tensile Fracture Surface, S-200-E (10^{-4}/sec)

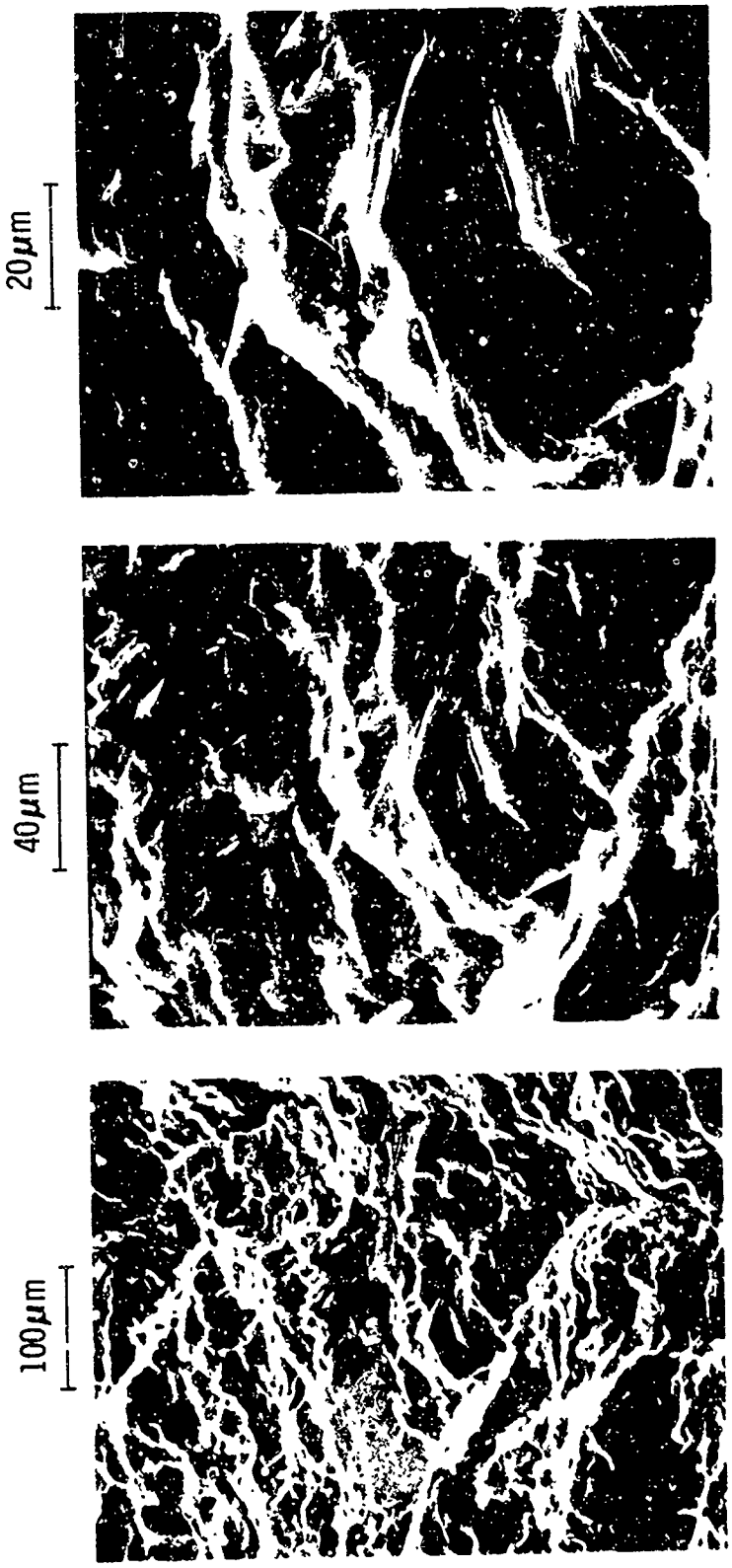

Figure 17 Spall Fracture Surface, S-200-E

MSL-71-23

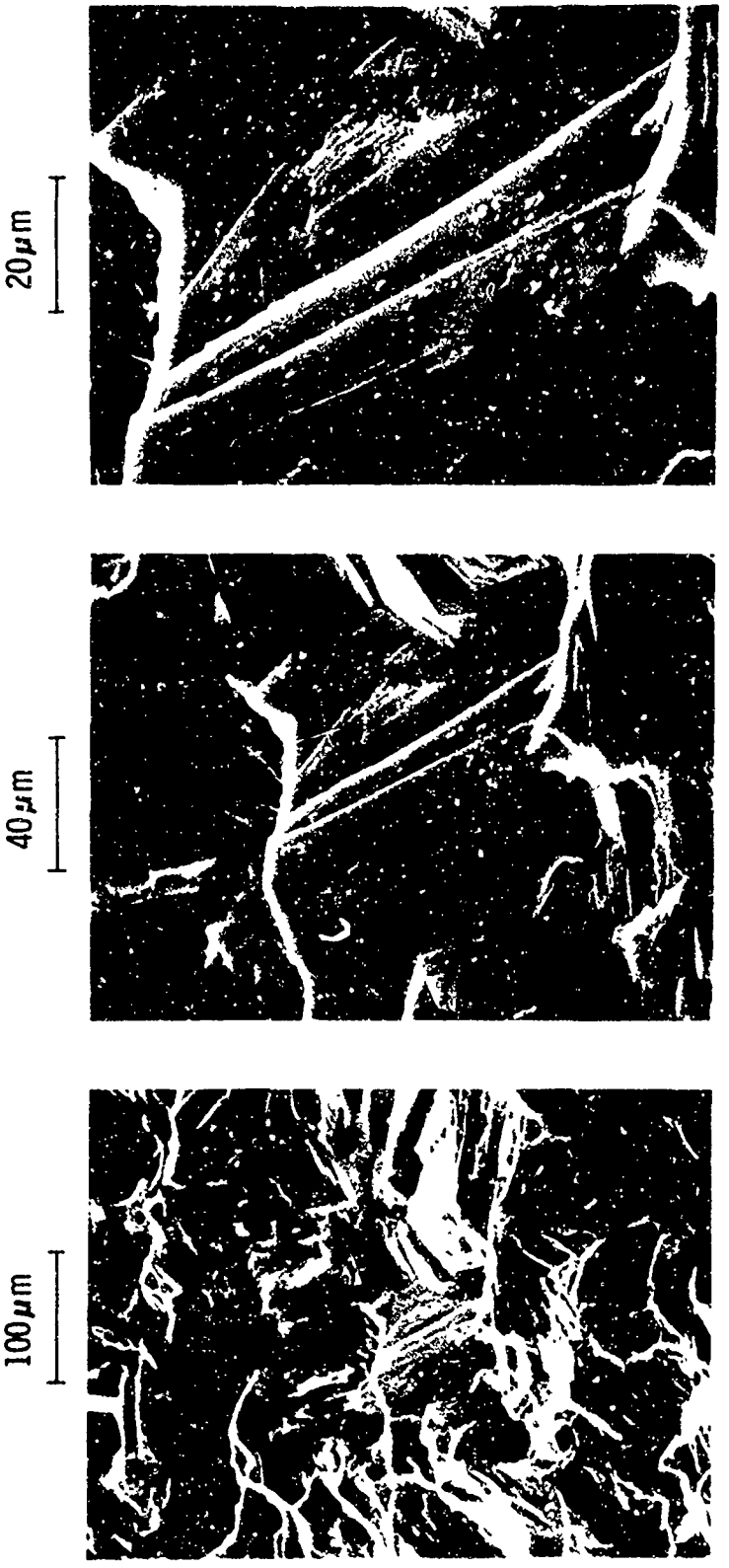

Figure 18 Spall Fracture Surface, High-Purity

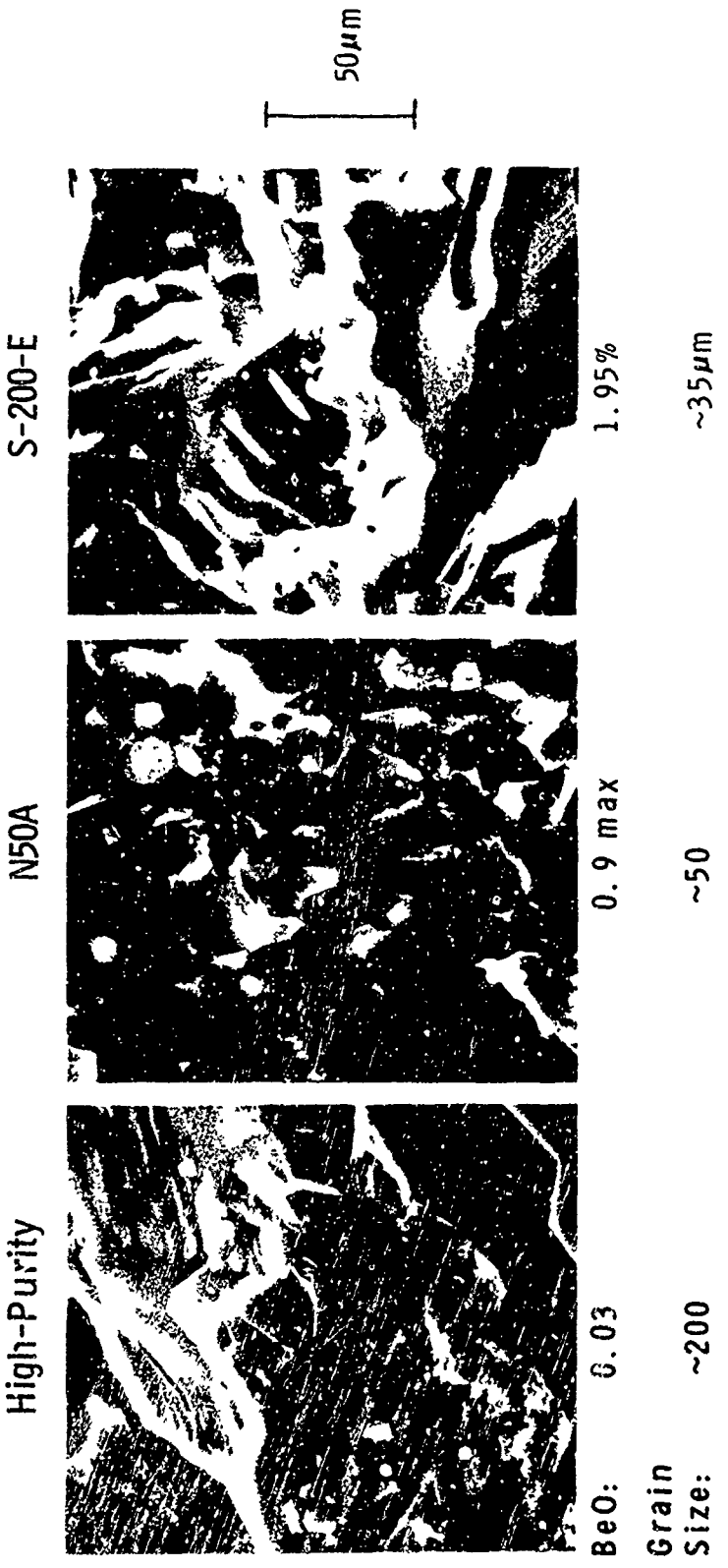

Figure 19 Fracture Surfaces, Beryllium

MSL-71-23

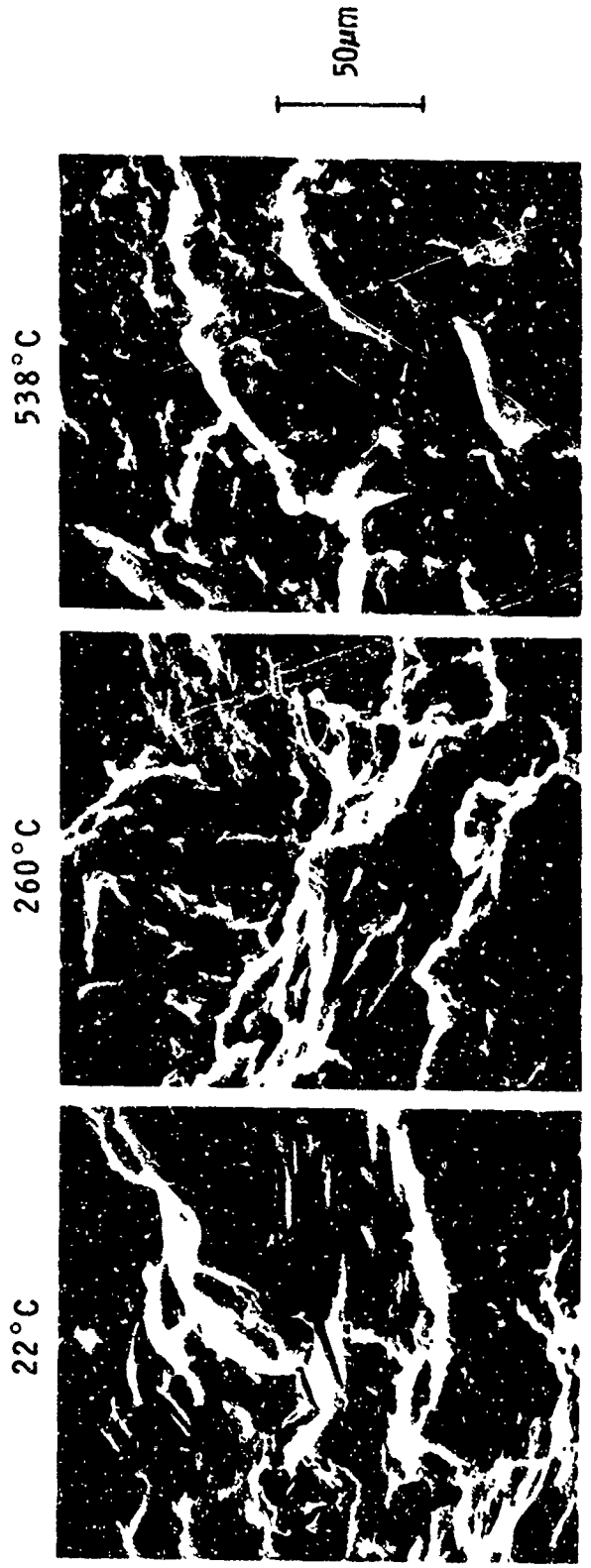

Figure 20 Fracture Surfaces, Temperature Effects, S-200-E

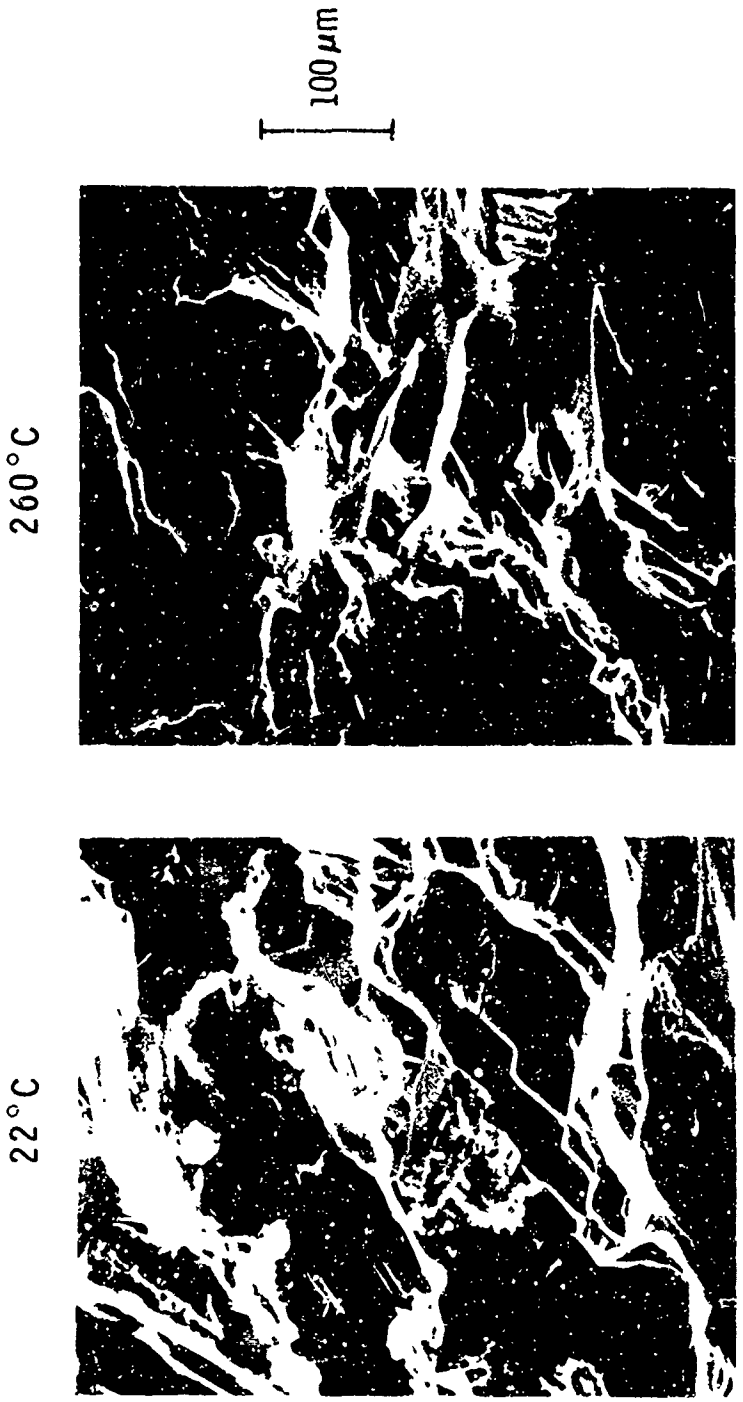

Figure 21 Fracture Surfaces, Temperature Effects, High-Purity

ACKNOWLEDGMENTS

The assistance of the following General Motors Corporation, Manufacturing Development, Materials and Structures Laboratory personnel in the experimental work is gratefully recognized: Mr. B. Bielski and Mr. J. Wigton for specimen preparation; Mr. F. Stemczynski and Mr. E. Miller for EOS and wave profile tests; Mr. J. Havens for ultrasonics measurements; Mr. H. Simmons for uniaxial stress tests; Mr. C. Whitchurch and Mr. L. Seltz for metallographic work; and Mrs. W. Trippen for data analysis.

REFERENCES

1. Isbell, W. M., Christman, D. R., Babcock, S. G., Michaels, T. E. and Green, S. J., "Measurements of Dynamic Properties of Materials, Vol. I: Summary of Results", General Motors Corporation, Manufacturing Development, DASA 2501-1, 1970 (AD 712847).

2. Christman, D. R., Isbell, W. M., Babcock, S. G., McMillan, A. R. and Green, S. J., "Measurements of Dynamic Properties of Materials, Vol. III: 6061-T6 Aluminum", General Motors Corporation, Manufacturing Development, DASA 2501-3, 1971.

3. Christman, D. R., Michaels, T. E., Isbell, W. M. and Babcock, S. G., "Measurements of Dynamic Properties of Materials, Vol. IV: Alpha Titanium", General Motors Corporation, Manufacturing Development, DASA 2501-4, 1971.

4. Christman, D. R., Isbell, W. M. and Babcock, S. G., "Measurements of Dynamic Properties of Materials, Vol. V: OFHC Copper", General Motors Corporation, Manufacturing Development, DASA 2501-5, 1971 (AD 728846).

5. Isbell, W. M., Christman, D. R. and Babcock, S. G., "Measurements of Dynamic Properties of Materials, Vol. VI: Tantalum", General Motors Corporation, Manufacturing Development, DASA 2501-6, 1971.

6. Christman, D. R., "Dynamic Properties of Poly(methylmethacrylate) (PMMA)", General Motors Corporation, Manufacturing Development, MSL-71-24, 1971.

7. Christman, D. R., Isbell, W. M., Babcock, S. G., McMillan, A. R. and Green, S. J., "Measurements of Dynamic Properties of Materials, Vol. II: Experimental Methods and Techniques", General Motors Corporation, Manufacturing Development, DASA 2501-2, 1971 (AD 730750).

8. Silversmith, D. J. and Averbach, B. L., "Pressure Dependence of the Elastic Constants of Beryllium and Beryllium-Copper Alloys", Phys. Rev. B, Vol. 1, p. 567-571, 1970.

9. Voronov, F. F. and Vereshchagin, "The Influence of Hydrostatic Pressure on the Elastic Properties of Metals. I. Experimental Data", Phys. Met. & Metall., Vol. 11, p. 111-118, 1961.

10. Baldwin, M. P., "The Measurement of the Elastic Moduli of Beryllium by an Ultrasonic Resonance Technique", United Kingdom Atomic Energy Authority, AWRE-049/70, August, 1970.

11. Gschneidner, K. A., "Physical Properties and Interrelationships of Metallic and Semimetallic Elements", Solid State Physics, Vol. 16, p. 275-426, 1964.

12. Thermophysical Properties of High Temperature Solid Materials, Vol. 1: Elements, Touloukian, Y. S., Ed., The McMillan Co., New York, N. Y., 1967.

13. Aerospace Structural Metals Handbook, Chapter Code 5101 (Be, Comm. Pure), Mechanical Properties Data Center, Belfour Stulen Inc., Traverse City, Michigan, 1963.

14. Hausner, H. H., Ed., The Beryllium Metal Handbook, General Astrometals Corp., New York, N. Y., 1967.

15. Taylor, A. and Kagle, B. J., Crystallographic Data on Metals and Alloy Structures, Dover Publications, Inc., New York, N. Y., 1963.

16. Kumble, R. G., Schierloh, F. L. and Babcock, S. G., "Mechanical Properties of Beryllium at High Strain Rates", General Motors Corporation, Manufacturing Development, SAMSO TR-68-71, Vol. VI, January, 1968 (AD 853914L).

17. Green, S. J. and Schierloh, F. L., "Uniaxial Stress Behavior of S-200 Beryllium, Isotropic Pyrolytic Boron Nitride, and ATJ-S Graphite at Strain Rates to 10^3/second and 700°F", General Motors Corporation, Manufacturing Deevelopment, MSL-68-11, March, 1968.

18. Schierloh, F. L. and Babcock, G. G., "Tensile Properties of Beryllium at High Strain Rates and Temperatures", General Motors Corporation, Manufacturing Development, AFML TR-69-273, October, 1969 (AD 865380).

19. Schemenski, R. M. and Maringer, R. E., "Microstrain Characteristics of Isostatically Hot-Pressed Beryllium", J. Less-Common Metals, Vol. 17, p. 25-45, 1969.

20. Abey, A. E. and Stromberg, H. D., "Shear Strength of Beryllium, Uranium, and Tungsten as a Function of Strain, Strain Rate and Pressure", ASME Trans.-J. Basic Eng., Series D, Vol. 93, p. 291-295, 1971.

21. Lindholm, U. S. and Yeakley, L. M., "Effect of Strain Rate, Temperature and Multiaxial Stress on the Strength and Ductility of S-200-E Beryllium and 6Al-4V Titanium", Southwest Research Institute, AFML TR-71-37, March, 1971 (AD 884041).

22. Conrad, H. and Cooke, F. W., "The Effects of Temperature and Strain Rate on the Strength of Beryllium Sheet", Met. Trans., Vol. 2, p. 1307-1313, 1971.

23. Inoue, N., Damiano, V., Hanafee, J. and Conrad, H., "Effects of Hydrostatic Pressure on the Mechanical Behavior of Polycrystalline Beryllium", AIME Trans., Vol. 242, p. 2081-2089, 1968.

24. Bunshah, R. F. and Armstrong, R. W., "The Dependence of the Hardness of Beryllium on Grain Size", Mat. Res. Bull., Vol. 4, p. 239-250, 1969.

25. Froula, N. H., "The Hugoniot Equation of State of S-200 Beryllium to 1000°F", General Motors Corporation, Manufacturing Development, MSL-68-16, July, 1968.

26. Christman, D. R., Froula, N. H. and Babcock, S. G., "Dynamic Properties of Three Materials, Vol. I: Beryllium", General Motors Corporation, Manufacturing Development, MSL-68-33, Vol. I, November, 1968; also, AIAA J., Vol. 8, p. 477-482, 1970.

27. Isbell, W. M., Shipman, F. H. and Jones, A. H., "Hugoniot Equation of State Measurements for Eleven Materials to Five Megabars", General Motors Corporation, Manufacturing Development, MSL-68-13, December, 1968 (AD 721920).

28. Munson, D. E., "Dynamic Behavior of Beryllium", Sandia Laboratories, SC-RR-67-368, June, 1967.

29. McQueen, R. G., Marsh, S. P., Taylor, J. W., Fritz, J. N. and Carter, W. J., "The Equation of State of Solids from Shock Wave Studies", High-Velocity Impact Phenomena, p. 293-417, Academic Press, New York, N. Y., 1970.

30. Davison, L. W. and Johnson, J. N., "Elastoplastic Wave Propagation and Spallation in Beryllium: A Review", Sandia Laboratories, SC-TM-70-634, September, 1970.

31. Conrad, H. and Perlmutter, I., "Beryllium as a Technological Materials", The Franklin Institute and the Air Force Materials Laboratory, AFML TR-65-310, November, 1965 (AD 477776).

32. Gilman, J. J., "Dislocation Dynamics and the Response of Materials to Impact", Appl. Mech. Rev., Vol. 21, p. 767-783, 1968.

33. Read, H. E., Triplett, J. R. and Cecil, R. A., "Dislocation Dynamics and the Formulation of Constitutive Equations for Rate Dependent Plastic Flow in Metals", Systems, Science, and Software, DASA 2638, December, 1970 (AD 722314).

34. Taylor, J. W., "Stress Wave Profiles in Several Metals", Dislocation Dynamics, p. 573-589, McGraw-Hill Book Co., New York, N. Y., 1968.

35. Warnica, R. L., "Spallation Thresholds of S-200 Beryllium, ATJ-S Graphite and Isotropic Boron Nitride at 75°F, 500°F and 1000°F", General Motors Corporation, Manufacturing Development, MSL-68-18, July, 1968.

36. Warnica, R. L., "Spallation Thresholds of N50A Beryllium", General Motors Corporation, Manufacturing Development, MSL-68-1, February, 1968.

37. Isbell, W. M. and Christman, D. R., "Shock Propagation and Fracture in 6061-T6 Aluminum from Wave Profile Measurements", General Motors Corporation, Manufacturing Development, DASA 2419, April, 1970 (AD 705536).

APPENDIX A

SPECIFICATION SHEETS

MSL-71-23

THE BRUSH BERYLLIUM COMPANY
17876 St. Clair Ave. • Cleve., O. 44110 • Phone: 486-4200 (Area: 216) • TWX: 421-8828 (Area: 810)

SPECIFICATION SHEET

QMV® BERYLLIUM BLOCK
STANDARD GRADES S-100-E AND S-200-E

Effective October 2, 1967

1. Scope

1.1 This specification defines the requirements for two standard grades of QMV® Beryllium designated as S-100 and S-200. In addition, two types within each grade are defined on the basis of radiographic quality.

These standard grades are produced by hot pressing beryllium powder. This specification covers parts and shapes that are machined from hot pressed material.

2. Chemical Composition

2.1 Chemical composition shall conform to the following:

	S-100-E	S-200-E
Beryllium Assay, % min.	98.5	98.0
Beryllium Oxide, % max.	1.2	2.0
Aluminum, % max.	0.14	0.16
Carbon, % max.	0.15	0.15
Iron, % max.	0.16	0.18
Magnesium, % max.	0.08	0.08
Silicon, % max.	0.08	0.08
Other Metallic Impurities % each, max.	0.04	0.04

2.2 Detailed analytical procedures used by The Brush Beryllium Company are available on request.

3. Density

3.1 The minimum bulk density shall be 1.84 grams per cubic centimeter.

3.2 Density shall be determined by using the water displacement method.

4. Tensile Properties

4.1 Minimum transverse* tensile properties at room temperature shall be:

	S-100-E	S-200-E
Ultimate Tensile Strength, psi, minimum	35,000	40,000
Yield Strength (0.2% offset) psi, minimum	27,000	30,000
Elongation (% in 1 inch) minimum	1%	1%

* Transverse with respect to the direction of pressing.

4.2 Test methods ASTM E8-61T and Fed. Test Method Std. No. 151 are applicable. Detailed test procedures used by The Brush Beryllium Company are available on request.

5. Penetrant Inspection

5.1 Liquid penetrant inspection of machined surfaces shall reveal no porosity or cracks.

5.2 Liquid penetrant inspection shall be performed in accordance with MIL-I-6866 A, Type 1 using penetrants and a dry developer conforming to MIL-I-25135 Group V. Personnel performing this inspection shall be certified in accordance with MIL-STD-410.

6. Radiographic Inspection

6.1 Radiographic indications (voids and/or inclusions) shall conform to the requirements as established and defined below:

6.1.1 Requirements:

Both grades of material shall conform to the requirements defined in 6.1.2 as follows:

Type	Maximum Dimension	Maximum Average Dimension	Total Combined Volume Per Cubic Inch
Type I	0.030 inch	0.020 inch	Sphere 0.050 inch diameter
Type II	0.030 inch	0.020 inch	Sphere 0.032 inch diameter

6.1.2 Definitions:

6.1.2.1 Maximum Dimensions of any Indication. Any dimension of any indication measured in the plane of the radiograph shall not exceed 0.030 inch.

6.1.2.2 Maximum Average Dimension of any Indication. The average dimensions of an indication shall not exceed 0.020 inch. The average dimension of an indication shall be the arithmetic average of the maximum and minimum dimensions measured in the plane of the radiograph.

6.1.2.3 Total Combined Volume Per Cubic Inch of all Indications. The total combined volume per cubic inch of all indications with an average dimension larger than 0.001 inch shall not exceed the volume of a sphere of the indicated diameter.

6.2 Radiographic inspection to a penetrameter sensitivity of 2% shall be performed in accordance with MIL-STD-453.

7. Grain Size

7.1 The average grain size shall not exceed 25 microns.

7.2 The average grain size shall be determined in accordance with ASTM E-112, Section 7b.

8. Tolerances

8.1 Material furnished under this specification shall conform to the dimensions and dimensional tolerances established by the purchase order and applicable drawings. If tolerances are not specified by the purchase order the following standard tolerances shall apply.

Diameter, Width or Thickness, Inches	Tol. Inch
Up to 3, inclusive	-0 + 1/64
Over 3 to 20, inclusive	-0 + 1/16
Over 20	-0 + 1/4
Length, Inches	
Up to 20, inclusive	-0 + 1/8
Over 20	-0 + 1/4

9. Surface Finish

9.1 The material shall be furnished with a machined surface. The standard surface finish shall be 125 microinches rms maximum.

10. Reports

10.1 Certification of compliance with this specification will be furnished on request and, when specified, actual test results will be certified. Testing in accordance with individual customer instructions will be performed if mutually acceptable and actual test results will be certified.

10.2 A report, in triplicate, containing the following information shall be furnished for each shipment.

Purchase Order Number
Material Specification Number
Part Number
Quantity Shipped

11. Marking

11.1 Each part, surface area permitting, will be legibly marked to give the following information:

Specification Number
Lot and/or Part Number
Manufacturer's Identification

APPENDIX B

WAVE PROFILES

(VELOCITY INTERFEROMETER)

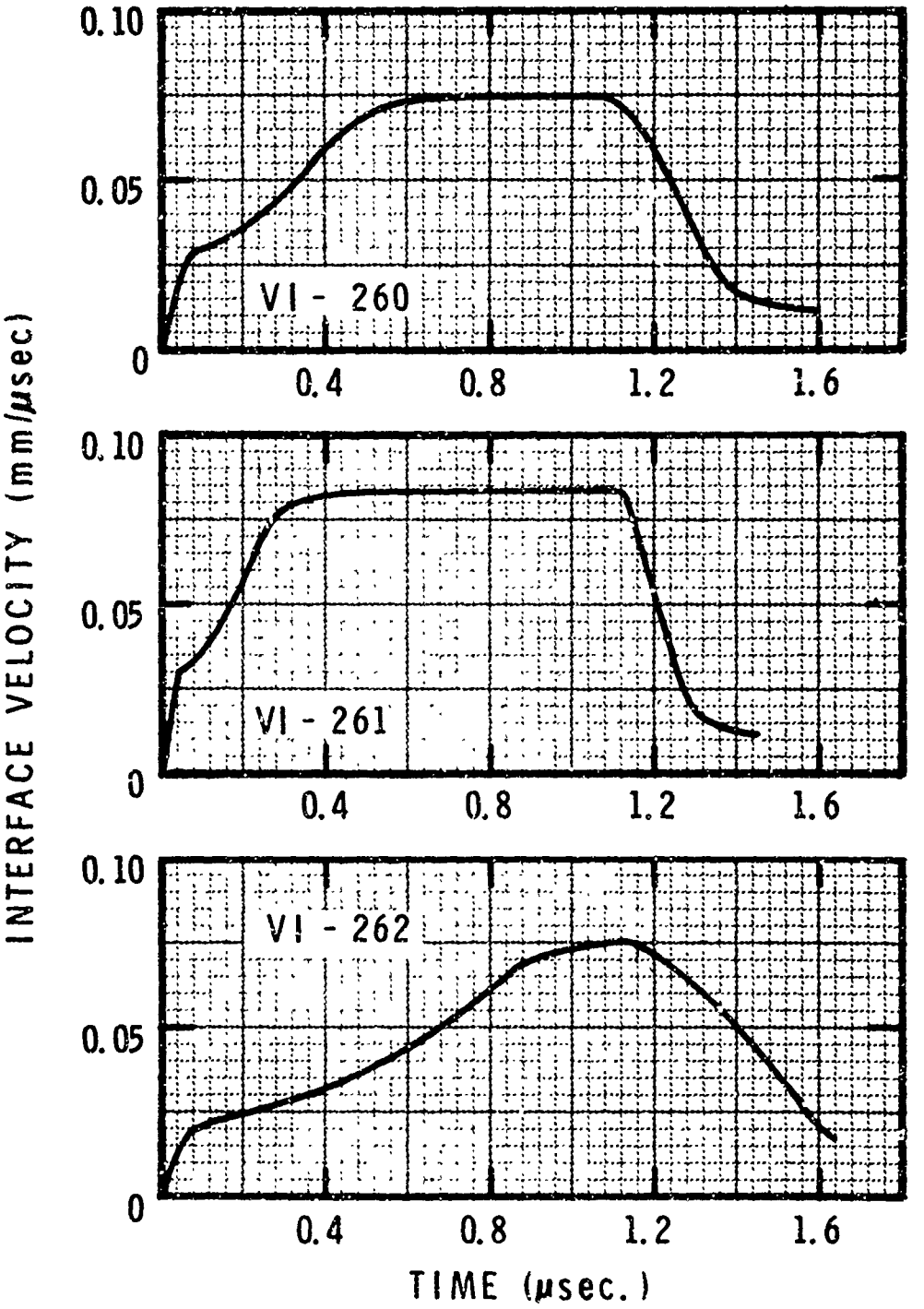
0.10
0.05
0
VI - 260
0.4
0.8
1.2
1.6
0.10
0.05
0
VI - 261
0.4
0.8
1.2
1.6
0.10
0.05
0
VI - 262
0.4
0.8
1.2
1.6
INTERFACE VELOCITY (mm/μsec)
TIME (μsec.)

MSL-71-23

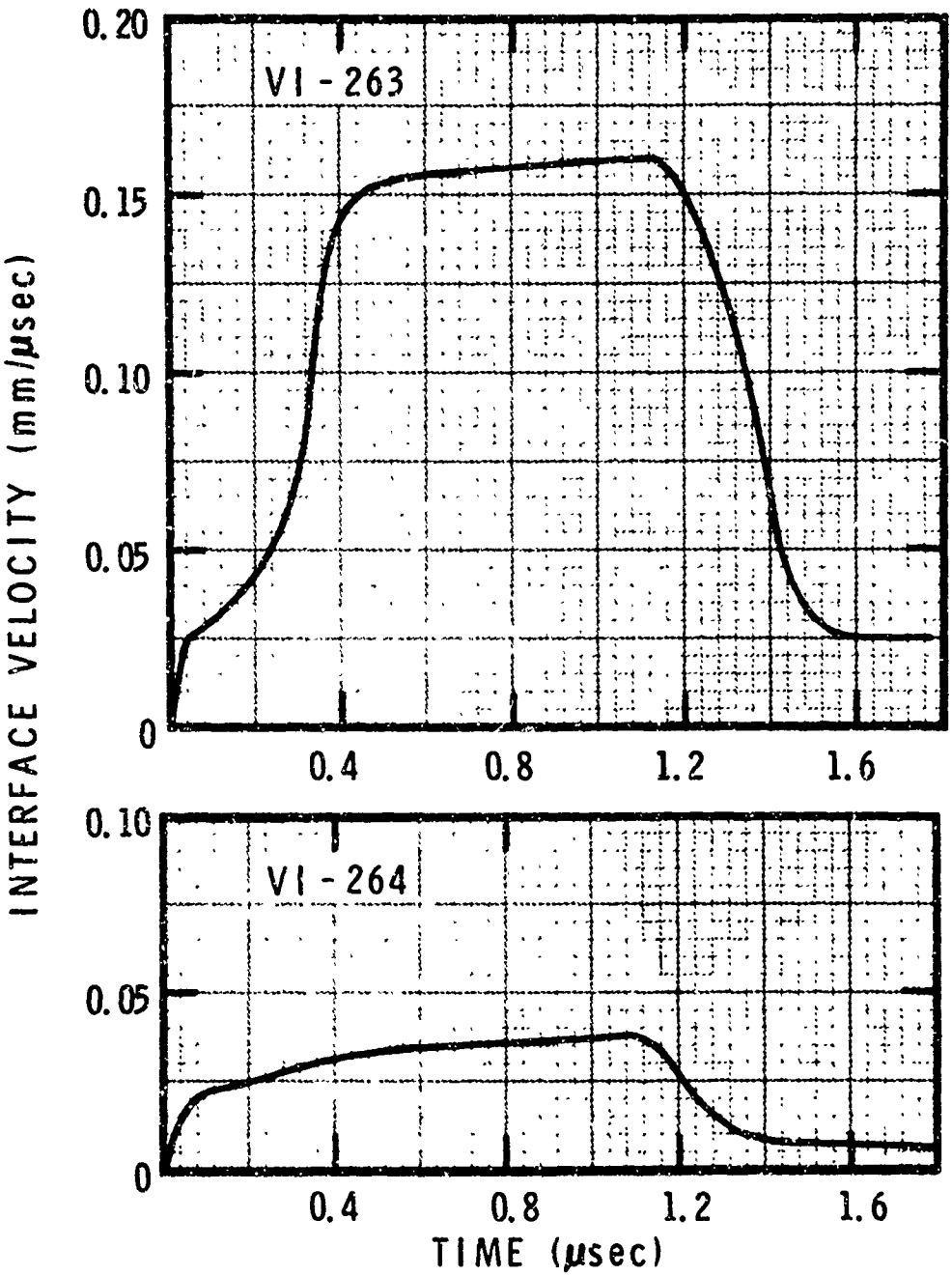
VI - 263
VI - 264
INTERFACE VELOCITY (mm/μsec)
TIME (μsec)
0.20
0.15
0.10
0.05
0
0.4
0.8
1.2
1.6

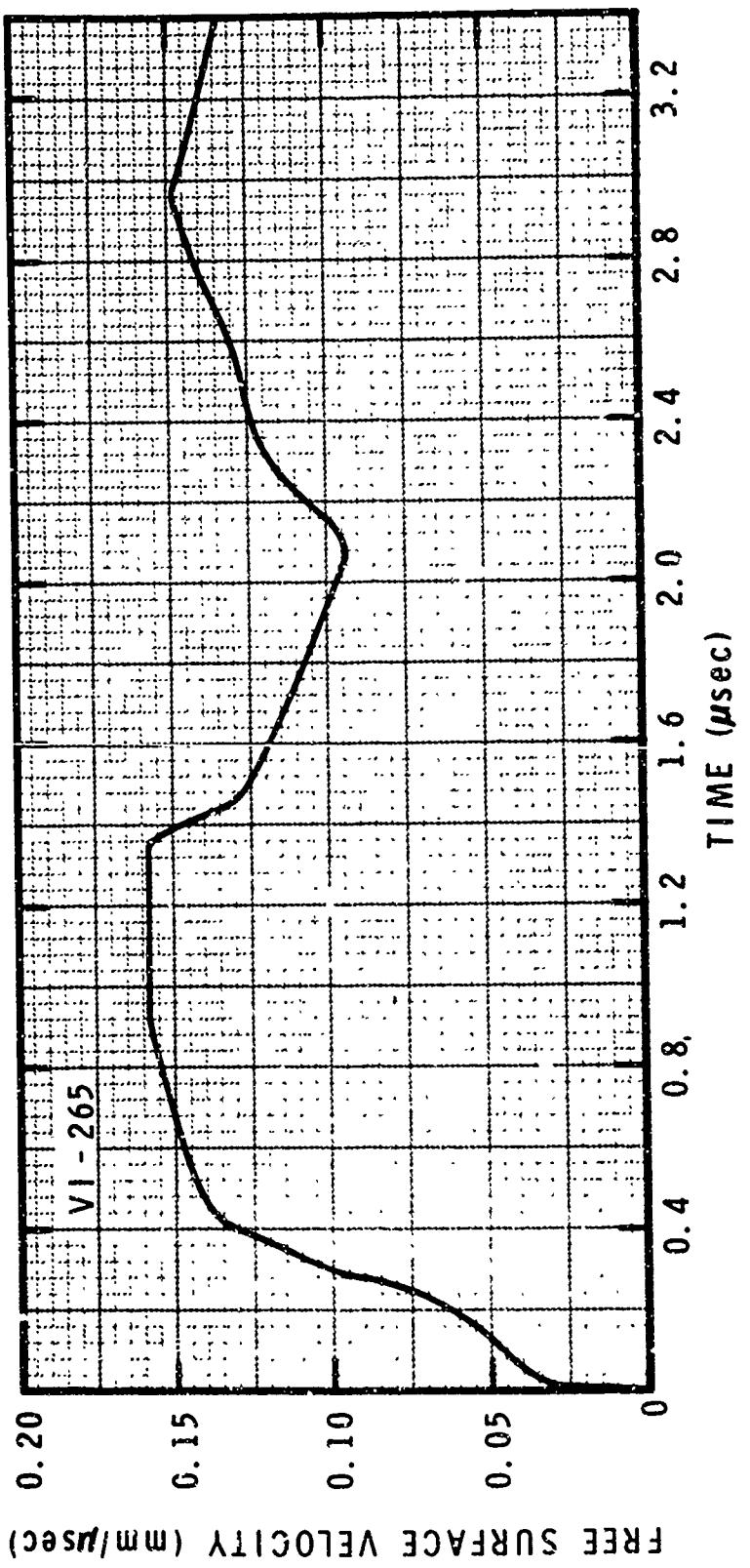
VI - 265
FREE SURFACE VELOCITY (mm/μsec)
0.20
0.15
0.10
0.05
0
0.4
0.8
1.2
1.6
2.0
2.4
2.8
3.2
TIME (μsec)

MSL-71-23

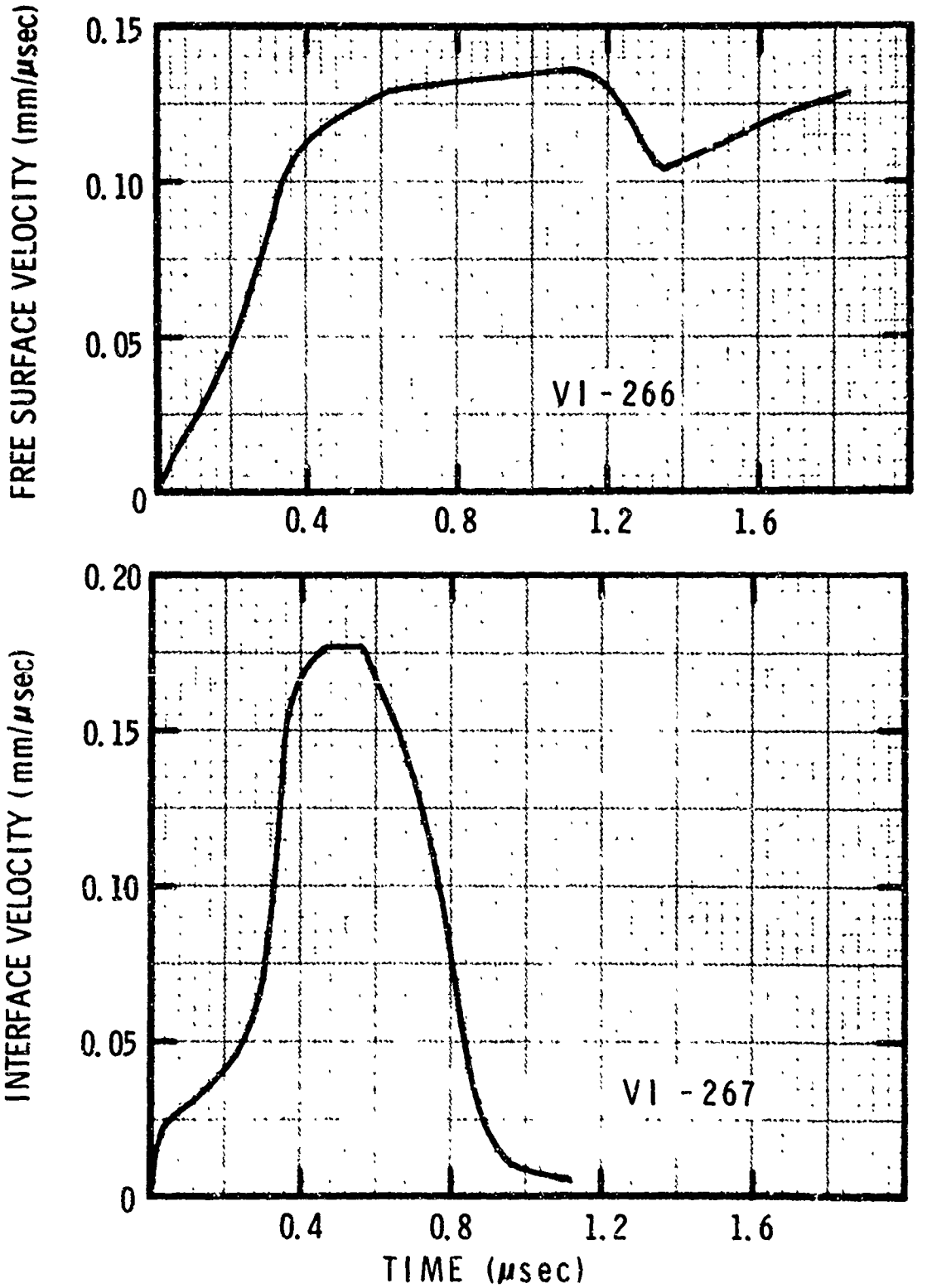
FREE SURFACE VELOCITY (mm/μsec)
0.15
0.10
0.05
0
VI - 266
0.4
0.8
1.2
1.6
INTERFACE VELOCITY (mm/μsec)
0.20
0.15
0.10
0.05
0
VI - 267
0.4
0.8
1.2
1.6
TIME (μsec)

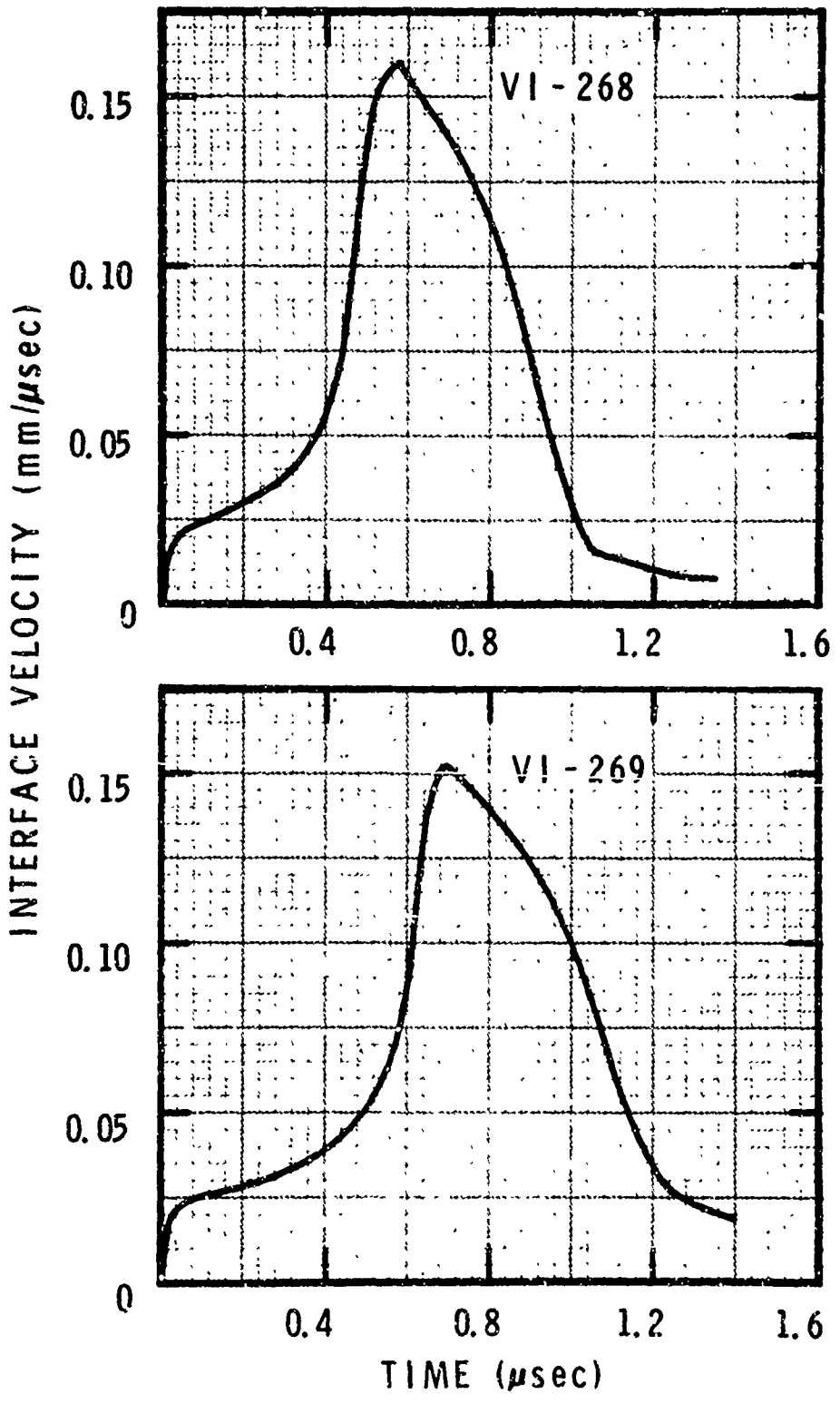
VI - 268
VI - 269
INTERFACE VELOCITY (mm/μsec)
0.15
0.10
0.05
0
0.4
0.8
1.2
1.6
TIME (μsec)